Icarus 220 (2012) 348–368

Contents lists available at SciVerse ScienceDirect

Icarus

journal homepage: www.elsevier.com/locate/icarus

Widespread crater-related pitted materials on Mars: Further evidence for the role of target volatiles during the impact process

Livio L. Tornabene [a,*], Gordon R. Osinski [a], Alfred S. McEwen [b], Joseph M. Boyce [c], Veronica J. Bray [b], Christy M. Caudill [b], John A. Grant [d], Christopher W. Hamilton [e], Sarah Mattson [b], Peter J. Mouginis-Mark [c]

[a] University of Western Ontario, Centre for Planetary Science and Exploration, Earth Sciences, London, ON, Canada N6A 5B7
[b] University of Arizona, Lunar and Planetary Lab, Tucson, AZ 85721-0092, USA
[c] University of Hawai'i, Hawai'i Institute of Geophysics and Planetology, Mānoa, HI 96822, USA
[d] Smithsonian Institution, Center for Earth and Planetary Studies, Washington, DC 20013-7012, USA
[e] NASA Goddard Space Flight Center, Greenbelt, MD 20771, USA

ARTICLE INFO

Article history:
Received 28 August 2011
Revised 29 April 2012
Accepted 9 May 2012
Available online 24 May 2012

Keywords:
Mars, Surface
Cratering
Impact processes
Geological processes
Terrestrial planets

ABSTRACT

Recently acquired high-resolution images of martian impact craters provide further evidence for the interaction between subsurface volatiles and the impact cratering process. A densely pitted crater-related unit has been identified in images of 204 craters from the Mars Reconnaissance Orbiter. This sample of craters are nearly equally distributed between the two hemispheres, spanning from 53°S to 62°N latitude. They range in diameter from ~1 to 150 km, and are found at elevations between −5.5 to +5.2 km relative to the martian datum. The pits are polygonal to quasi-circular depressions that often occur in dense clusters and range in size from ~10 m to as large as 3 km. Pit sizes scale with both the host crater's diameter and the host deposit size. These pits have subtle raised rims, and unlike primary and secondary impact craters, they lack well-defined ejecta deposits and overlapping stratigraphic relationships. They also lack any sign of any preferential alignment expected of volcanic or tectonic collapse features. Morphologic and stratigraphic evidence in support of an impact origin includes the observation that pitted materials primarily occur as ponded and flow-like deposits on crater floors, behind terraces, and infilling the lowest local topographic depressions atop the ejecta blanket—similar to the distribution of impact melt-bearing bodies on the Moon. Based on the observations and comparisons to terrestrial and lunar analogs, we conclude that the pit-bearing materials are impactite deposits. The presence of these deposits in older craters, where preserved, suggests that they have formed on Mars throughout most of its geologic history; thus, understanding their origin may help to constrain the hydrological and climate history of Mars.

1. Introduction

Impact craters are among the most recognizable landforms on almost all solid bodies in our Solar System. Although they have consistent gross morphologic attributes (e.g., a cavity, raised-rim, ejecta), they can be morphologically diverse. This diversity often reflects the effect of the target properties on the impact process (e.g., Melosh, 1989), but also post-impact climatic and active geologic processes that commonly modify craters. Hence, pristine crater morphology can be used as a standard to understand target material properties (e.g., Stewart and Valiant, 2006; Boyce and Garbeil, 2007), and the effects and rates of subsequent modifying processes on Mars (e.g., Craddock et al., 1997; Bleacher et al., 2003; Forsberg-Taylor et al., 2004; Grant et al., 2008). In addition, pristine craters offer us a glimpse of the relatively unmodified primary crater deposits, provide insights into the impact cratering process itself, and potentially paleo-environments, especially on planetary bodies that are more complex due to the presence of an atmosphere and target volatiles (e.g., water).

This study documents the existence of widespread crater-related pitted materials (e.g., Fig. 1) associated with both interior and exterior deposits of pristine and well-preserved impact craters. Pitted materials often occur with other notable features, such as various types of flows, channels, dissected deposits and alluvial fan-like features, all of which have been described in previous studies (e.g., Morris et al., 2010; Williams and Malin, 2008; Jones et al., 2011). Although previously recognized in some craters (McEwen et al., 2005; Tornabene et al., 2006; Mouginis-Mark and Garbeil, 2007; Preblich et al., 2007; Hartmann et al., 2010; Morris et al., 2010), these crater-related pitted materials have not been characterized on a global scale and over a range of crater diameters. Here, we describe the occurrence and morphology of crater-related pitted materials, note stratigraphic relationships with crater-related

* Corresponding author. Fax: +1 519 661 3198.
E-mail address: ltornabe@uwo.ca (L.L. Tornabene).

0019-1035/$ - see front matter © 2012 Elsevier Inc. All rights reserved.
http://dx.doi.org/10.1016/j.icarus.2012.05.022

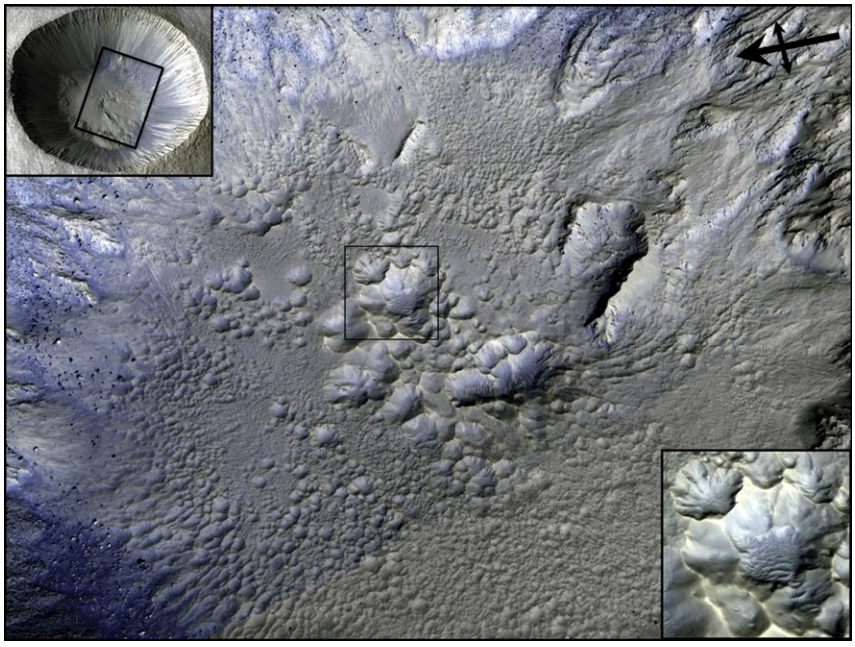

Fig. 1. Crater-related pitted materials observed on the floor (i.e., the crater-fill) of Zumba Crater in Daedalia Planum (see Fig. 14 for context). This 3D perspective view was generated by draping the combined full resolution (25.2 cm/pixel) orthorectified HiRISE RED and IRB color composite image on a 1 m per post HiRISE stereo pair-derived DTM (DTEEC_002118_1510_003608_1510_A01). The view is 1:1 with no vertical exaggeration. The scale of features depends on where you look in the perspective, but the pitted crater-fill deposits (not including slumps and talus deposits) is roughly circular and ~1.1 km in diameter. Talus, debris flows and other mass wasted materials (boulders) sourced from the crater walls superpose the pitted materials. (Lower right inset) This image shows a ~2× close-up of some of the largest pits in IRB color. Aeolian bedforms (bluer) are apparent on the floors of pits. The smooth pit walls (lighter-tones) may possess coatings, dust or are potentially comprised of ferrous-bearing phases (Delamere et al., 2010). The semi-isolated pit with the "spur and gully" morphology in the upper left inset is ~50 m in diameter. Image/data credits: NASA/JPL/UA. (For interpretation of the references to colour in this figure legend, the reader is referred to the web version of this article.)

features and other deposits, measure various morphometric attributes using high-resolution Digital Terrain Models (DTMs), and constrain the timing of its emplacement with respect to the impact event. This study also provides a global database of pitted material-bearing craters to assess the occurrence of pitted materials as function of latitude, elevation, preservation, target type, ejecta type, central feature type, and thermophysical properties. These relationships, or lack thereof, provide insights into the formation and emplacement processes for the pitted materials.

In this paper, craters described as "pristine" refer specifically to a class of craters that are Late Amazonian in age and also possess sharp, relatively unmodified morphological features (e.g., crater rim, terraces, central uplift). Minimal infilling, morphologically and thermophysically distinctive ejecta, in addition to the presence of very small and very few overprinting impact craters, further characterize a pristine crater. The large rayed craters reported in Tornabene et al. (2006), but also Tooting Crater (Mouginis-Mark and Garbiel, 2007) and Gasa Crater (Schon et al., 2009; Schon and Head, 2011), are excellent examples of this class. Craters described as "well-preserved" in this paper refer specifically to Amazonian and Hesperian-aged craters that have most of their morphologic features intact, but show multiple overprinting impacts, and varying degrees of erosion, degradation, burial, and in some cases, exhumation. The distinctions between "pristine" and "well-preserved" made in this study generally require high-resolution images (meter-scale or better). It should be noted that these classes have some overlap, however they differ from the preservation classes reported by Barlow (2004), which were characterized with coarser resolution datasets, and did not account for overprinting impacts.

2. Background

Prior to the acquisition of Mars Reconnaissance Orbiter (MRO) data (Zurek and Smrekar, 2007), pristine martian craters were studied using a variety of datasets, which included visible and thermal images and laser altimetry. The recognition of martian "thermal" rayed craters in nighttime thermal images from the Mars Odyssey (MO) Thermal Emission Imaging System (THEMIS) as a defining characteristic for crater "freshness" was particularly useful, yet these craters are only detected over surfaces with certain thermophysical properties, which accounts for only ~20% of the surface of Mars (McEwen et al., 2005; Tornabene et al., 2006; Preblich et al., 2007). Based solely on morphologic characteristics, Mouginis-Mark and Garbiel (2007) demonstrated that Tooting Crater, which lies outside of this thermophysical unit and lacks thermally detectable crater rays, is one of the most pristine craters of its size class. It was in these craters, both the "thermal" rayed craters and Tooting, in which the pitted materials were first recognized and documented. Mouginis-Mark and Garbiel (2007), using Mars Global Surveyor (MGS) Mars Orbiter Camera Narrow-Angle (MOC-NA; Malin and Edgett, 2001) images, reported on a pitted unit that occupies some of the lowest portions of the Tooting's crater floor, which they interpreted to be "a mantling unit of unknown origin that conformably overlies the impact melt sheet". Crater-related pitted materials were also recognized in MOC-NA images of two young rayed craters, the ~3 km diameter Zumba Crater (Tornabene et al., 2006) and the ~10 km diameter Zunil Crater (Preblich et al., 2007). However, MOC-NA images yielded insufficient coverage and detail for a comprehensive interpretation of their origins.

3. Datasets, derived data products, and methods

Images from MRO continue to provide the best quality and highest resolution data to evaluate fine-scale crater-related morphologic features in detail—including the crater-related pitted materials (McEwen et al., 2007b; Tornabene et al., 2007a, 2007b, 2008). These include sub-meter-scale High Resolution Imaging

Science Experiment (HiRISE; McEwen et al., 2007a, 2010) images and decameter-scale Context Imager (CTX; Malin et al., 2007) images. For most craters (especially those >50 km in diameter), one or more HiRISE (~25–32 cm/pixel) and/or CTX (~6 m/pixel) images (McEwen et al., 2007a, 2010; Malin et al., 2007) were often required to make a definitive identification of the presence of pitted materials. In addition, data and derived datasets from the MGS and MO missions were used to aid the identification and characterization of crater-related pitted materials. For example, lower spatial resolution visible images (i.e., MOC-NA [~3 m/pixel] and THEMIS-Visible [~18 m/pixel]) and thermal infrared images from THEMIS [~100 m/pixel]) (Malin and Edgett, 2001; Christensen et al., 2004) were sometimes adequate for the identification of pitted materials and determining their stratigraphic relationships.

The MGS Mars Orbiter Laser Altimeter (MOLA) Mission Experiment Gridded Data Records (MEGDRs; 128 pixel/deg or ~462 m/pixel), along with selected individual Precision Experiment Data Records (PEDRs; ~160 m footprint size, ~300 m along track spacing, ~0.37 m vertical precision) (Smith et al., 2001), were used in this study for morphometric measurements of key craters. Detailed meter-scale morphometric measurements were derived via analysis of three HiRISE stereo-derived DTMs: one for Zumba Crater (DTEEC_002118_1510_003608_1510), one for Corinto Crater (DTEEC_003611_1970_004244_1970) and one for Mojave Crater (DTEEC_001481_1875_002167_1880). HiRISE DTMs (1 m/pixel grid spacing) were produced using Integrated Software for Imagers and Spectrometers (ISIS) and SOCET Set (copyright BAE Systems). Their production, accuracy and precision are described in Kirk et al. (2008) and summarized in McEwen et al. (2010). Profile extractions from the HiRISE stereo-derived DTMs are based on qualitative assessments of shaded relief maps used in conjunction with orthographically rectified (orthorectified) HiRISE red mosaic images to: (1) visually identify problematic areas due to image jitter and Charge-Couple Device (CCD) seams, and (2) avoid shadowed, or extremely smooth and featureless areas. All DTM measurements and 3D perspective images were acquired and processed using the Environment for Visualizing Images (ENVI) software, and the HiRISE ENVI tool kit provided by ITT Visual Information Solutions in conjunction with the HiRISE operations team.

The Java Mission And Remote Sensing (JMARS) Geographical Information System (GIS) software for Mars (Gorelick et al., 2003; Christensen et al., 2009) was used to facilitate quick and easy access to multiple global datasets and to facilitate our global survey. JMARS was also used to compile a geospatial database of pitted material-bearing craters. Numeric datasets such as MOLA elevation, Dust Cover Index (DCI; Ruff and Christensen, 2002), albedo and thermal inertia (both of which are derived from the Thermal Emission Spectrometer (TES) data (Christensen et al., 2001)), were averaged and recorded for each crater in the database (see Table A.1).

4. Observations

4.1. Global distribution of crater-related pitted materials and age estimates of the host craters

Our preliminary study of craters from pole to pole (~82°N to 88°S) with HiRISE images resulted in two important and consistent observations that were vital with respect to defining a systematic survey: (1) pitted material preservation positively correlates with the host crater's preservation (i.e., the most pristine craters have the most pristine pitted materials), and (2) pitted materials do not occur in high latitude craters (>60°)—even in pristine examples (e.g., see Lonar Crater – 38.27°E, 73.03°N; Boyce et al., 2008). Using the global THEMIS nighttime thermal infrared (nTIR) brightness temperature mosaic and the global MOLA MEGDR shaded relief map, we suggested targets to both MRO-HiRISE and CTX for any craters between the latitudes of 60°N and 60°S that: (A) had a thermophysical contrast with their surroundings, typical of pristine and well-preserved craters, and/or (B) had a sharp appearance in the shaded relief map (i.e., well-defined crater rim, ejecta, terraces and central features). This resulted in a database of 1063 craters. Of 1063 craters examined, 784 craters (~73%) currently have sufficient visible image coverage and/or resolution to determine the presence of pitted materials. Pitted materials are observed in 204 (~26% of the 784) with possible detections in an additional 171 craters, which still require coverage with HiRISE for confirmation. The sample of pitted material-bearing craters spans the size range ~1–150 km in diameter, occurs over a wide range in latitude (~62°N to 57°S) and elevation (approximately −5.5 to +5.2 km) and are found within diverse target terrains that span all three periods martian geologic time (Fig. 2 and Table A.1 and 1).

Overall, pitted material-bearing craters do not show a strong preference for the northern vs. the southern hemisphere (94 and 110 in the north and south, respectively). However, a histogram of the number of pitted material-bearing craters per 10° latitude bin (normalized to bin area and scaled by a constant – 10^7) shows a distinctive bimodal distribution with respect to latitude (Fig. 2). The distribution shows 75% of our sample occurring in the lower mid-latitude regions of Mars (~10–30°N and °S), with fewer craters at or near the equator and a complete lack of them at high latitudes as previously discussed. Within the full sample population's latitude boundaries there are several areas that have few or completely lack pitted material-bearing craters, these include the Arabia Terra, Utopia Planitia and the interior of the Hellas Basin. There is a slight spike in the sample population between ~30° and 40°N, which appears to be attributed to a cluster in the Tharsis region. Overall, the pitted material-bearing craters also occur within a variety of target materials. To assess if there is a bias towards a specific terrain type, we normalized the pitted material-bearing crater population with respect to the area of generalized terrain types, which are based on the geologic unit descriptions of Scott and Tanaka (1986) and Greeley and Guest (1986). Results showed that these craters are found in all generalized terrain types (e.g., volcanic, heavily-cratered terrains, plains, etc.) and do not exhibit a strong preference for any specific terrain.

Pitted material-bearing craters exhibit a range of ejecta types and interior central morphologies (see Barlow et al. (2000) for a summary and description of ejecta types). Ejecta range from radial (Rd), diverse (Di) and single-, double- and multi-layered (SLE, DLE, MLE) types. Interior central morphologies include peaks, peak pits, central floor pits and complex morphologies (see Tables 2 and A.1). Overall, these craters appear to be nearly equally distributed between SLE, MLE, and Di ejecta types (Table 2). Craters with DLE and Rd ejecta are less common. These craters also show a slight preference to floor pit (including incipient floor pits), but they also commonly occur in craters with central peaks and peak pit central feature types. Note that the craters that show no central feature are simple or transitional craters (the largest of which is the 10.6 km diameter Ellsey Crater; see Table A.1).

A comparison of the pitted material-bearing crater population with surface thermophysical properties (Tables 3 and A.1), particularly the DCI map of Ruff and Christensen (2002), indicates that martian surface dust does not generally obscure pits. However, there is an apparent lack of pitted material-bearing craters in the Arabia Terra region (Fig. 2). Arabia Terra lacks pitted material-bearing craters when compared to other dust-covered regions (e.g., Elysium and Tharsis).

Thirty-five of the 204 craters (~17%) are suggested to be among the most pristine (youngest) craters in their size-class (Table 1). The remaining 163 pitted material-bearing craters (~83%) are

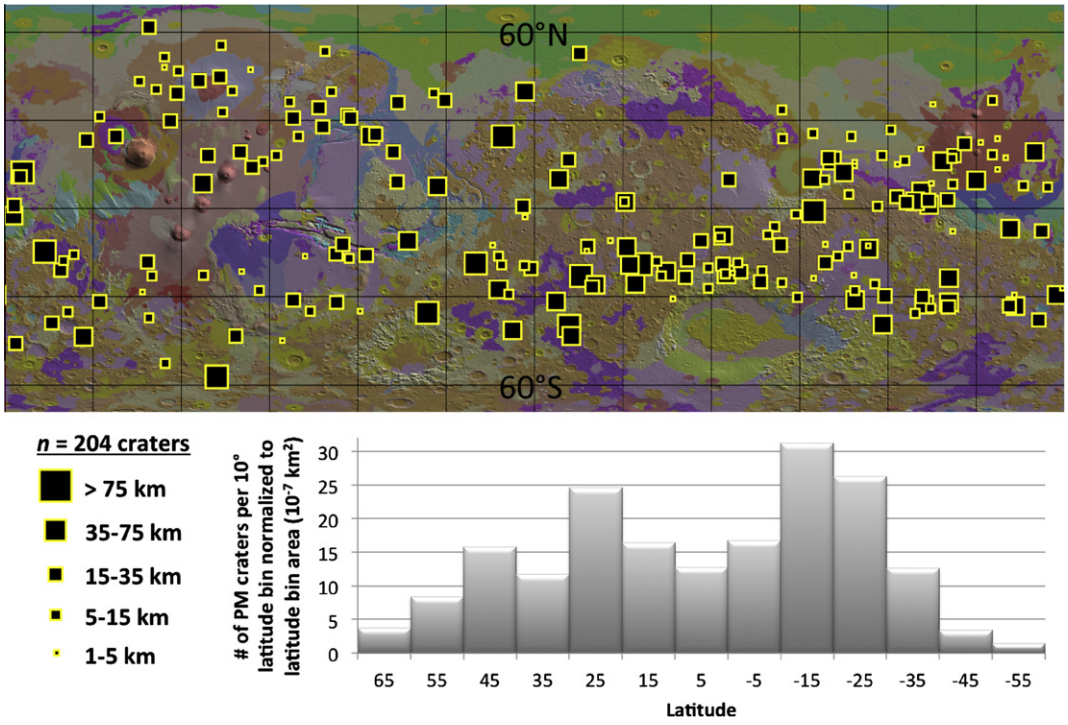

Fig. 2. A global distribution map of all currently identified pitted material-bearing craters ($n = 204$) ranging from ~1–150 km in diameter. The sample population is superimposed on the Skinner et al. (2006) digitized geologic map. (Bottom center) A histogram of the distribution of all 204 pitted material-bearing craters per 10° latitude bin and normalized to the latitude bin area and then scaled by a constant (10^7 km^2). Center line of longitude is 0°.

considered to be well-preserved craters that are partially eroded and buried, and perhaps even exhumed (Table A.1). The nearly equal distribution of these craters in the northern and southern hemispheres is consistent with a randomly distributed population of pristine and well-preserved craters, which should not show a preference to either hemisphere.

Our preservation classes are relative and qualitative; therefore, depth-to-diameter ratios (d/D) are presented to add quantitative support for the preservation state of these craters. Although influenced by target and impactor properties, a high d/D is generally indicative of minimal erosion and burial (e.g., Boyce et al., 2006; Boyce and Garbeil, 2007). Thirty-one craters (7 simple and 24 complex) were chosen from our database based on crater preservation and their spread with respect to diameter over the range of our sample of pitted material-bearing craters, and MOLA PEDR coverage and viewing geometry (i.e., the size and location of the MOLA footprint with respect to the rim and crater floor). The d/D measurements were based on the maximum rim elevation and the lowest floor elevation, including central floor pits when applicable. Fig. 3 shows that all seven simple craters fall on or above the d/D scaling estimate range derived from Garvin et al. (2003). Of the 24 complex craters plotted here, three fall at or above the Boyce and Garbeil (2007) derived estimates for complex craters, representing the possible maximum d/D for a given crater size bin. Nineteen (~79%) fall above the scaling estimate from Garvin et al. (2003), representing global averages for complex craters. Six craters fall below and are shallower than the estimated average depths of both Garvin et al. (2003) and Boyce and Garbeil (2007). Shallower depths may not be from subsequent modification, but can arise due to the inherent limitations of the MOLA PEDR dataset with respect to the spacing and spot size of the laser on the surface and the feature of interest (e.g., in this case, the highest crater rim crest and the lowest spot on the crater floor; see discussions in Stewart and Valiant (2006) and Boyce and Garbeil (2007)). However, all six of the overly shallow craters occur at moderate to high latitudes (~30–60°N and °S), where higher concentrations of ground ice and/or very active seasonal and periglacial activity are expected (e.g., Clifford, 1993; Pathare et al., 2005; Clifford et al., 2010), which may explain their shallower depths.

Additional quantitative evidence for crater age may be derived from the Size–Frequency Distributions (SFDs) of superimposed impact craters (e.g., Hartmann, 2005, 2010). A modeled crater retention age, based on SFDs of superimposed craters, demonstrates that several pitted material-bearing craters (Table 1) are quite young, Late Amazonian-aged craters (~0.1–30 Ma; Hartmann et al., 2010; Schon and Head, 2011). The Hartmann et al. (2010) results confirm that some of these craters may represent the most-recently formed crater of a given size class, as first suggested by McEwen et al. (2005). This is inferred by comparing the crater retention age of a crater of size X with the expected reoccurrence interval of formation for a crater of size X (see Table 1 in Hartmann et al. (2010)). Overall, our observations of craters containing pitted materials suggest that the best-preserved examples of pitted materials also occur within what are qualitatively and quantitatively young, and well-preserved craters.

4.2. Pits: general characteristics and morphometry

In this section, we describe the general characteristics of the pits. Overall, observations of pits from the most pristine craters are generally consistent. Individual pits are distinctive negative-relief features with quasi-circular to or polygonal shaped cavities that are partly infilled with fine-grained materials (e.g., Fig. 1). They are also relatively shallow and possess only subtle raised rims (often completely lacking them at the limits of HiRISE resolution). The pits do not appear to possess proximal ejecta materials, as would be expected for overprinting impact craters. Even in the freshest craters, the pits have varying degrees of cover by dust and wind-blown materials, which can cause slight variations in their appearance from crater to crater. This is best illustrated in

Table 1
Thirty-five pristine and well-preserved pitted material-bearing craters (D = 1–140 km) and the martian "lunar-like" Pangboche crater.

Name[a]	Age[b] (Myr)	D (km)	Long° (E)	Lat° (N)	HiRISE	Stereo/ DTM	CTX	Unit ID[c]	Central feature	Ejecta type	Ejecta ponds	Terrace ponds	d_m (km)[e]	%Deeper[f]
"Scandia"	n.d.	18.9	229	61.7	18758_2420	Y/N	P19_008341_2420	Aa1	Peak pit	MLE	No	No	1.58	3.9
Maricourt	n.d.	9.2	288.85	53.33	7851_2335	Y/N	P15_006981_2335	Aa1	Peak pit	MLE	No	Yes	1.15	7.4
"Alba3"	n.d.	14	234.41	51.41	16490_2315	Y/N	P16_007339_2309	Hal	Pit	MLE	No	Smooth	1.13	−15.9
"Alba2"	n.d.	21.2	253.02	44.62	6745_2250	Y/N	P15_006745_2270	Aau	Pit	SLE	Smooth?	Yes	2.01	19.9
"Alba1"	n.d.	10.8	231.66	40.52	16345_2210	Y/N	B18_016701_2208	Hal	Incip. Pit	SLE	Smooth?	Yes	1.15	−0.7
"Utopia"	n.d.	14.6	84.14	33.49	9164_2140	Y/N	P21_009098_2138	Aps	Peak pit	MLE	Maybe	Yes	1.27	−5.1
Canala	n.d.	11.2	279.92	24.35	10370_2045	Y/N	P16_007377_2030	Hr	Pit	SLE	Yes	Yes	1.21	2.6
Tooting	0.8–10	28.2	207.78	23.18	1538_2035	Y/N	P01_001538_2035	Aa3	Peak	MLE	Yes	Yes	2.16	14.3
"Elysium minor"	n.d.	2.5	151.44	22.48	9333_2025	Y/N	P07_003637_2002	Ael1	None	Rd	No	n/a	0.54	18.9
"Ascraeus"	n.d.	19.6	260.07	19.28	4134_1995	Y/N	P07_003844_1994	At5	Pit	MLE	Yes	Yes	1.6	3.5
"Elysium major"	n.d.	38.9	169.89	19.26	7447_1995	Y/N	P16_007447_1984	Ael1	Peak pit	MLE	No	No	2.39	9.3
Thila	n.d.	5.1	155.54	18.11	9346_1985	Y/N	P21_009346_1983	Ael1	Pit	Rd	No	n/a	0.89	11.4
*Pangboche	n.d.	10.3	226.61	17.28	1643_1975	Y/N	P02_001643_1974	Aos	Incip. Pit?	Rd	No	Smooth	1.19	5.3
Corinto	2–8	13.5	141.72	16.95	3611_1970	Y/Y	P07_003611_1971	Ael1	Pit	SLE	Yes	Yes	1.31	1.3
Tomini	2–30	7.8	125.89	16.27	1871_1965	Y/N	P02_001871_1964	Hr	Pit	SLE	No	n/a	1.22	19.1
Nayrn	4–31	4	123.3	14.89	1660_1950	Y/N	P02_001660_1950	Ahpe	Incip. Pit	Rd	Yes	Smooth?	0.65	1.4
Dilly	n.d.	2.1	157.23	13.27	6841_1935	Y/N	B01_010203_1934	Ael1	None	Rd	Yes	n/a	0.4	3.5
"Isidis"	n.d.	47.5	94.31	10.19	8689_1905	Y/N	P16_007107_1897	Aps	Peak pit	Di	Smooth?	Yes	2.66	10.2
"Hypanis"	n.d.	16.3	313.4	8.95	9393_1890	Y/N	P19_008536_1890	Npl2	Pit	SLE	No	No	1.52	7.1
Zunil	0.06–1	10.4	166.19	7.7	1764_1880	Y/N	P02_001764_1877	Aps	Peak	MLE	Yes	Yes	1.23	7.9
Mojave	n.d.	56.8	327	7.5	1481_1875	Y/Y	P03_002167_1877	Hchp	Peak	MLE	Yes	Yes	2.73	4.7
"Sabaea"	n.d.	1	17.74	−14.64	7044_1650	NO	P15_007044_1632	Npld	None	Rd	No	n/a	0.37	42.9
"Sinai"	n.d.	1.5	281.98	−16.26	14405_1635	Y/N	B17_016172_1630	Hr	None	Rd	Yes	Yes	n.d.	n.d.
Gratteri	0.5–20	7.2	199.95	−17.71	10373_1620	Y/N	P01_001367_1621	Nplr	Peak pit	SLE	Maybe	Maybe	0.99	4.2
"Tyrhenna"	n.d.	34.4	98.74	−18.48	8544_1615	Y/N	P16_007252_1629	Npld	Peak pit	MLE	maybe	Yes	2.6	21.6
Noord	n.d	7.8	348.74	−19.27	7757_1605	Y/N	P17_007757_1611	Npld	None	SLE	yes	Yes	1.07	7.8
"Hesperia minor"	n.d.	6.9	115.68	−25.79	7436_1540	Y/N	P16_007436_1539	Hr	Incip. Pit	SLE	eroded?	n/a	0.97	4
Resen	n.d.	7.6	108.88	−27.94	4008_1520	Y/N	P18_008135_1518	Hr	Incip. Pit	SLE	yes	n/a	0.97	−0.6
Zumba	0.1–1	2.8	226.93	−28.67	3608_1510	Y/Y	P03_002118_1512	Ht2	Incip. Pit	Rd	yes	n/a	0.64	24.5
"Hesperia major"	n.d.	73.3	108.72	−31.29	11761_1485	Y/N	B01_009849_1485	Hr	Peak	Di	maybe	Yes	2.91	−1.5
Horowitz	n.d.	63.1	140.77	−32.04	10006_1475	Y/N	B01_010006_1475	Npld	Peak	Di	eroded	Eroded?	2.93	6.2
"Sirenum"	n.d.	11.2	201.63	−35.4	13208_1445	Y/N	B05_011573_1443	Npld	Pit	SLE	no	Maybe	1.25	5.6
Gasa	n.d.	7.2	129.41	−35.72	4060_1440	Y/Y	P08_004060_1440	Npl1	None	Di	smooth	n/a	n.d.	n.d.
Hale	n.d.	138.5	323.58	−35.65	Multiple	Y/N	P05_002932_1445	Nplh	Peak	Di	yes	Yes	5.34	24.4
"Aonia"	n.d.	4.6	274.19	−45.1	7127_1345	Y/N	P15_006837_1331	Hpl3	None	Di	yes	Yes	0.81	11.2
"Sirenum south"	n.d.	10.4	234.68	−52.87	12574_1270	NO	B07_012429_126	Npl1	Pit	SLE	maybe	Yes	1.07	−6.2

[d] Ejecta type (e.g., Barlow et al., 2000) – Single Layer Ejecta (SLE), Double Layer Ejecta (DLE), Multi-Layered Ejecta (MLE), Rd – Radial ejecta and Di – Diverse.
[a] Some unnamed craters are referred to by their regional location, or by a noted geographical landmark (e.g., Hesperia = Hesperia Planum; Olympus = Olympus Mons) in quotation marks.
[b] Age based on Table 1 in Hartmann et al. (2010); Tooting age from Mouginis-Mark and Boyce (2012) is consistent with the Hartmann ranges.
[c] Geologic unit based on the Skinner et al. (2006) digitized geologic map after Scott and Tanaka (1986) and Greeley and Guest (1986).
[e] Based on MOLA PEDRs and/or MEGDRs (see text).
[f] % Difference based on the MOLA measured depth vs. the estimated depth based on Garvin et al. (2003); positive values denote craters that are deeper than the Garvin estimate.

crater-to-crater comparisons made with HiRISE color Infrared–Red–Blue/green (IRB) images. These show that the pit floors often contain common and readily recognizable aeolian bedforms. This is corroborated by observations of pit walls and floors that are distinct in color, suggestive of differences in composition (Delamere et al., 2010). In rare cases, where the pits are well-exposed and relatively free from surface deposits, outcrops containing meter- to decameter-sized light-toned rounded to angular rock fragments can be observed outcropping in the pit walls (Fig. 4). The observation that these breccias are outcropping in the walls of pits, and not a deposit that sits atop the pits, are supported by observations with HiRISE stereo-derived anaglyphs.

Pits can be solitary, or they can occur as a large pit surrounded by a dense collection of relatively smaller pits (Fig. 5). These "solitary" pits tend to be more circular and exhibit an inner spur and gully morphology associated with their walls; whereas pits that have significant overlap with other pits of a similar size, tend to be polygonal to irregular in shape and form relatively shallower "faceted" inner walls (Fig. 1). The walls of either solitary or clustered pits are distinctive with respect to slopes. They notably possess shallower outer portions and steeper inner portions, which can be perceived in non-stereo images, but is best observed in anaglyphs, 3D perspective images and profiles extracted from HiRISE stereo pairs (Figs. 5 and 6). The outer, relatively shallower slope

Table 2
Ejecta and central feature characteristics of all 204 pitted-material bearing craters.

Ejecta type[a]	#	%	Central feature type[b]	#	%
Buried[b]	2	1.0	Complex	6	2.9
DLE	4	2.0	Incipient pit	19	9.3
Rd	27	13.2	None	25	12.3
Di	44	21.6	Peak pit	46	22.5
MLE	57	27.9	Peak	49	24.0
SLE	70	34.3	Pit	59	28.9
Total	204			204	

[a] After Barlow martian crater database 1.5 (Barlow et al., 2000).
[b] Lavas emplaced after crater formation nearly or completely covering the ejecta blanket.

Table 3
Statistics on the average km-scale themophysical characteristics of all 204 pitted-material bearing craters.

	TES DCI[a]	TES Albedo[b]	TES TI[b]
Max.	0.984	0.321	486
Min.	0.850	0.109	46
Mean	0.959	0.194	208
Mode	0.969	0.244	239
Median	0.963	0.178	227
Std. dev.	0.017	0.059	81

[a] TES Dust Cover Index values of 0.960 and higher are considered to be relatively dust-free surfaces with values lower than this typically representing surfaces that are spectrally and thermophysically dominated by the presence of dust and other surface fines; low values of DCI correlate well with high albedos and lower TI consistent with this interpretation (Ruff and Christensen, 2002).
[b] See Christensen et al. (2001).

portion of the pit wall (~15–20° as measured in the DTMs) extends out from the rim to an abrupt break in slope ~0.25–0.5R_p (where R_p = pit radius), at which the wall becomes steeper (>25°) towards the inner portion of the pit cavity. This overall profile shape in Figs. 5 and 6 appears to be consistent regardless of the size of the pits.

Some pits appear to have raised rims in non-stereo images. However, observations from HiRISE anaglyphs and DTMs (McEwen et al., 2010) indicate that many are not true positive relief features. By comparing single image to stereo image observations, we suggest that the appearance of a raised rim is due to pit overlap and observation geometry. In both anaglyphs and DTM profiles, these apparent rims consistently fall below the surface level of the host unit (e.g., Fig. 6). Essentially, the pits are incised into their host materials and although the pits may have subtle deposits associated with them, these deposits generally do not protrude above the local datum defined by the surface of the surrounding host material.

Both pit size and density are observed to increase locally within an individual crater with respect to the area of the host deposit (e.g., pond size/area). The largest pits are always found within the crater-fill deposit with successively smaller pit sizes observed within pit-bearing materials found within the wall–terrace region and ejecta blanket. Measurements of average pit size from various locations within the ~28 km Tooting Crater (Fig. 7) show that the average pit diameter generally drops off exponentially with radial distance from the center of the crater, or with respect to location (i.e., crater-fill, terrace ponds or ejecta deposits). This suggests that pit size is generally a function of the area (more likely the volume and thickness) of the pit-bearing host unit with the largest pits typically being observed within the central portions of a unit (i.e., where the deposit may, in fact, be thickest). The largest pits are also sometimes observed along edges, margins or contacts between the pit-bearing host unit and the faulted and displaced bedrock within a crater (e.g., crater wall rock, terrace blocks, central uplifts). Pit size also is observed to vary within an individual pitted unit (e.g., Fig. 1), and not all surfaces within a contiguous unit have dense pit clusters.

Pits consistently increase both in size and number as a function of increasing crater diameter. Fig. 8 shows a general trend for both the maximum pit diameter (D_{mp}) and the average pit diameter (D_{ap}) of the 10 largest crater-fill pits from the 13 freshest pitted unit-bearing craters. These trends are best fit by power laws with a R-squared value of 0.947 and 0.985, respectively. The equations are:

$$D_{mp} = 27.5D_c^{0.86} \quad (4.2.1)$$

where D_{mp} is the maximum pit diameter (i.e., largest pit) in meters and where D_c is the host crater's diameter in kilometers; and

$$D_{ap} = 16.4D_c^{0.87} \quad (4.2.2)$$

where D_{ap} is the average of the 10 largest pit diameters in meters. It should be noted that Fig. 8 includes both central peak and central floor pit craters. However, the above equations are based only on the central peak craters (n = 9). Central floor pit craters generally fall above the trend line, which suggests that the size of crater-fill pits may be influenced by central feature type (i.e., a larger volume of pitted deposit is accommodated by the lack of a central peak) or, if pit formation is related to the impact process, the target-types or conditions that are conducive to central floor pit formation.

The presence of pitted materials can be difficult to prove in older, well-preserved craters due to the more frequent occurrence of superimposed craters, erosion and infilling. Landforms that are consistent with being remnant pits are recognizable in over 160 craters (Table A.1), based on their similar morphology to the pitted materials observed in the most pristine craters (Table 1). In addition to these qualitative similarities, the trends in pit size (above) can be used to test putative pit structures observed in older craters. For example, Thila Crater (Table 1) shows what appear to be several remnant pit structures ~70–80 m in diameter. Using Eqs. (4.2.1) and (4.2.2), a crater the size of Thila is predicted to produce pits that average ~70 m, and a pit as large as ~110 m in diameter. Therefore, based on the correlation between the estimates and the measurement of the putative pit structures in Thila, in addition to their qualitative similarity to fresher pits in craters of similar size, we are confident that these features are indeed remnant pits.

4.3. Pitted materials

Here two main morphologic units that host the pits are distinguished: (1) the ponded unit, which are defined by their relatively level quasi-equipotential surfaces and occurrence in local topographic lows, and (2) a flow-like unit that emanates from and connects higher elevation ponded units with lower elevation ones including the lowest lying pitted materials of the crater-fill deposits. In the following sections, additional detailed morphologic, morphometric and stratigraphic relationships for each of the two occurrences of pitted materials are presented to gain insight into the origin and emplacement of the host unit and the pits themselves. These pitted materials are distributed amongst three crater settings, described below.

4.3.1. Crater floors

Pitted materials occurring as part of the crater-fill are the largest, most extensive, and most commonly recognized crater-related pitted unit. Crater-fill pitted materials are observed in pristine simple craters as small as a kilometer in diameter, and typically occupy a small portion of the crater-fill (up to ~0.007 km^2 or ~6% for 1 km diameter crater). At slightly larger diameters, as small as ~1.5 km, the pits are observed to pervade the entire extent of crater-fill

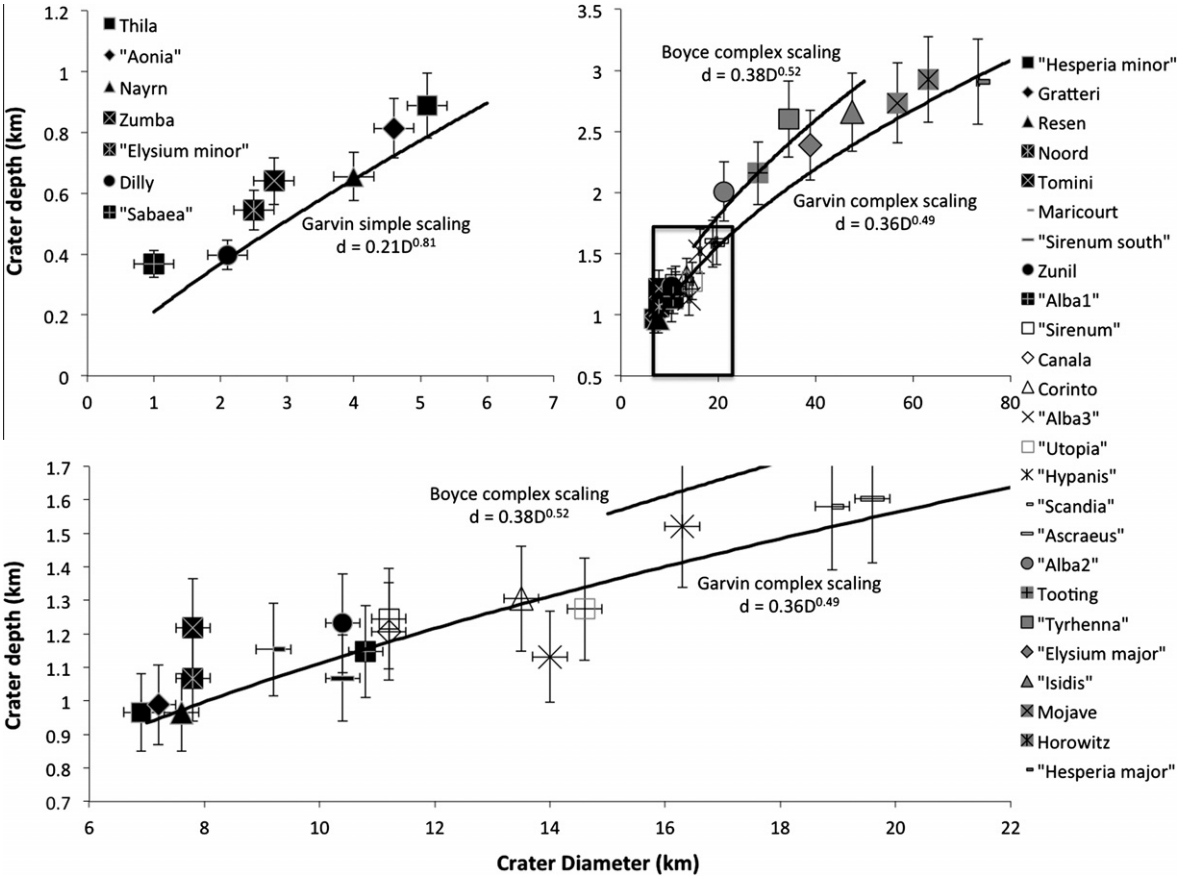

Fig. 3. Thirty-one depth-to-diameter ratios (d/D) for the best-preserved pitted-material-bearing simple to complex craters identified in our study (see Table 1). The black trend-lines in all three panels represents estimated d/D scaling, "Garvin" and "Boyce", based on Garvin et al. (2003) and Boyce and Garbeil (2007). (Top left) Simple crater d/D vs. the "Garvin" d/D scaling for simple craters D = 1–6 km. (Top right) Complex crater d/D vs. both "Garvin" and "Boyce" scaling for complex craters D = 7–80 km. The black box outlines the graph at the bottom of this figure. (Bottom) Close-up view of d/D for complex craters D = 7–20 km. Overall, six craters are ~0.7–16% shallower than the "Garvin" relationship while the remaining craters are ~1.3–43% deeper than average. Error bars are based on the resolution limits of THEMIS (for D) and the resolution and geometry limits of the MOLA PEDRs (for d) (for more on d/D error bars see Stewart and Valiant, 2006; Boyce and Garbeil, 2007).

deposit; however, as crater diameter continues to increase, and crater morphology begins to transition from simple to complex, and the location and concentration of crater-fill pitted materials varies with respect to the type and extent of crater modification. This change in crater morphology from simple to complex appears to influence the spatial occurrence and density of pits within the crater-fill. For example, the most extensive sector of wall slumping appears to influence the location and concentration of pitted materials. An unnamed crater in Aonia Terra (D = 4.6 km; Fig. 10) and another in Gasa Crater (D = 7.2 km) (Table 1), both exhibit extensive slumping/terracing on the southern crater wall that appears to have influenced the occurrence of the pitted crater-fill materials. These craters appear to have isolated their pitted materials on the northern crater floor where the lowest crater floor elevations are observed and there are minimal effects from crater modification (i.e., slumping/terracing). An excellent example of pitted materials being influenced by crater modification can be seen in a 24 km unnamed complex crater in Valles Marineris (294.8°E, 12.3°S; see Table A.1 for more details). The extreme uneven slopes (downhill from S to N) near the floor of the canyon can be inferred to have modified the crater in such away that its floor is deepest on its north side (i.e., more terracing on the south and much less terracing on the north side), this is the portion of the crater that hosts the largest and densest pitted materials of the crater-fill deposits.

Most pitted materials possess intervening relatively smooth regions between the pits with the most densely pitted surfaces generally occurring within the central portions of the deposit and/or along the contact between pitted materials and bedrock of the central uplift and the crater wall/terraces. In some cases, fractures similar to those observed in large lunar craters (e.g., Tycho; see Heather and Dunkin (2003)), are also observed, but are only within large complex craters (>20 km in diameter). Also like lunar crater-fill fractures, the martian crater-fill fractures often form polygonal patterns with several examples of crosscutting concentric and radial fractures. Interestingly, pits are both crosscut by, but also in some cases overprint the fractures, suggesting that pit and fracture formation may have been contemporaneous (e.g., Fig. 4).

Pit sizes and population densities may be affected by the presence and type of central features in complex craters. In craters with topographic central peaks or peak pits, two basic relationships with the pitted materials can be observed: (1) the pitted materials embay or partially superimpose exposed bedrock of the central uplift, including examples of where the bedrock appears partially buried by the pitted materials and (2) dense concentrations of pits surround and/or radiate from uplift structures (e.g., fractures or possible faults). Craters with incipient or full formed central floor pits show distinctive relationships with pit size and density, including: (1) the crater central floor pit feature can be comprised or contain high densities of pitted materials, and in such cases these pits are the largest pits in the entire crater (e.g., see images of Resen and "Ascraeus" craters; refer to Table 1), or (2) dense concentrations of pitted materials surround the crater central floor pit

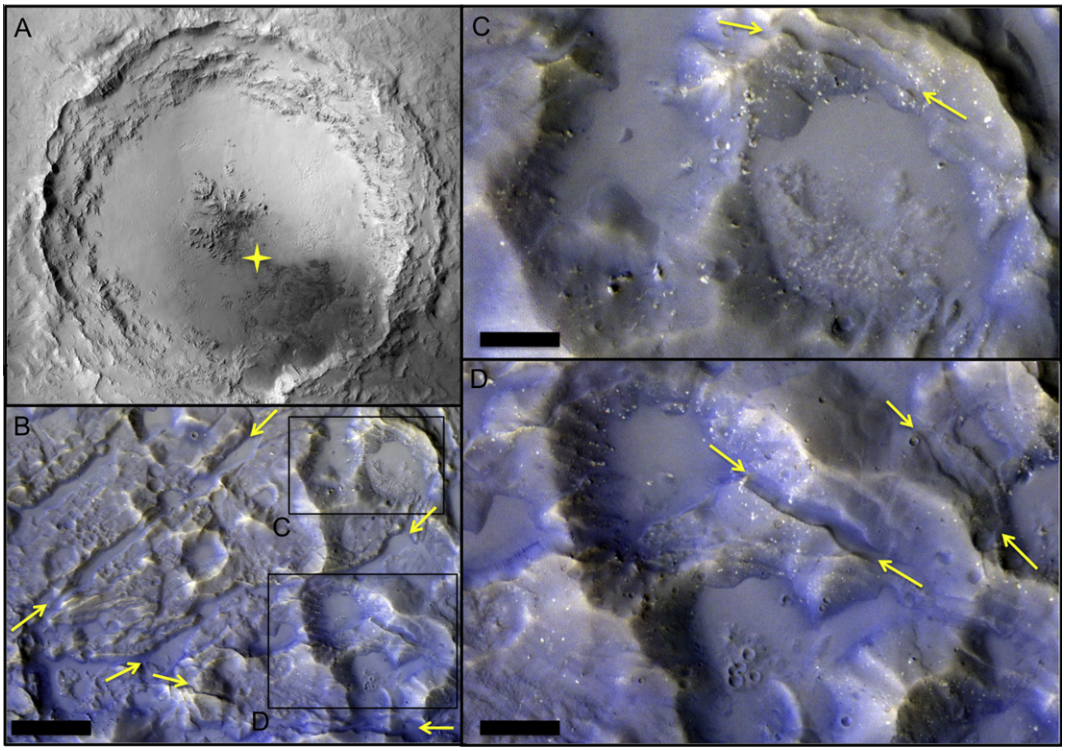

Fig. 4. Close-ups of the well exposed pitted materials observed on the floor of Mojave Crater. (A) A CTX mosaic of Mojave Crater showing the location of the well-exposed pits. The pits are well exposed only in this potion of crater, while elsewhere dust obscures most of Mojave Crater (consistent with thermophysical properties from TES (Christensen et al., 2001)). The approximate locations of images B–D are marked by the yellow star. (B–D) HiRISE IRB color images (PSP_002602_1875) of the well exposed pitted materials. Fractures that cross-cut and predate the pits are common within the pitted materials of complex craters and are marked here by yellow arrows. (C and D) Magnified views from (B) that show possible fragmental light-toned blocks outcropping within the walls of pits. The smallest resolvable blocks are ~1 meter across. Abundant fine-grained and relatively light-toned materials appear to partially fill the pit floors. Scale bars: (B) ~200 m; (C) ~60 m; (D) ~70 m. Image credits: NASA/JPL/MSSS and NASA/JPL/UA. (For interpretation of the references to colour in this figure legend, the reader is referred to the web version of this article.)

feature with fewer individual discernable pits occurring within the crater central floor pit feature (e.g., Corinto Crater). In addition, the data in Fig. 8 suggest that the average and maximum pit sizes are generally larger in craters with central floor pit features when compared to craters with central peaks or peak pits.

4.3.2. Wall/terraces

The next most distinctive occurrence of crater-related pitted materials is found within semi-enclosed topographic lows formed from the listric faulting that occurs within the rim–terrace region of some transitional (Fig. 10) and complex craters (Fig. 11). Fig. 9 shows the smallest transitional complex crater in our database (D = 4.6 km; "Aonia" Crater in Table 1), which exhibits the onset of terracing and the occurrence of these terrace ponds of pitted materials. Larger, more complex craters with well-formed terraces possess the most distinctive pitted terrace ponds. Tooting Crater possesses a well-formed terrace pond that is enclosed by the bedrock and the overall structure of a faulted terrace block on its northwest side (see Morris et al. (2010) and Mouginis-Mark and Boyce (2012, in press) and figures therein). Fig. 10 shows an additional example of ponded and pitted materials within the western terraces of Mojave Crater ($D \sim 57$ km; Table 1). Anaglyphs, profiles, and 3D perspectives of this and other examples indicate that they generally possess low-slope surfaces (<5°) with a slight dip towards the overall regional slope.

In addition to the pitted ponds, the crater terrace region also contains a flow-like unit. This unit is contiguous with the terrace ponds, as well as the pitted materials of the crater-fill (e.g., Fig. 9a–d). Observations of this flow-like unit in large complex craters such as Mojave Crater (see images listed in Table 1) suggest that they are sourced or emanate from the highest tier of ponded and pitted units and connect with lower elevation pitted materials (i.e., successively lower terraces) until they merge with the pitted materials of the crater-fill. These flows appear to be channelized by the terrace blocks until they ultimately merge with the crater-fill deposits. These channelized flows are similar to the "viscid flow fields" described by Williams and Malin (2008; see Figs. 3–5 and 7) in Mojave Crater. However, we note that Mojave preserves a complex set of other flow morphologies that appear to be unique to this crater, especially when compared to many of the pristine complex craters in this study. Mojave possesses two distinct types of flows: what we refer to here as "channelized flows" (e.g., Fig. 10) and "inviscid flow fields" (interpreted to be alluvial fans (Williams and Malin, 2008)). In almost all cases, the alluvial fans superpose the crater-related pitted materials (Tornabene et al., 2007b; Williams and Malin, 2008) and are never crosscut by pits or the pitted materials. The channelized flows in Mojave (also observed in Tooting Crater; Fig. 11) consist of up to three generations of pitted and non-pitted flows based on stratigraphic relationships. The non-pitted flows post-date both the pitted flows and pitted and ponded deposits, while pitted flows are contemporaneous with pitted and ponded deposits within the terraces and the crater-fill.

A CTX observation of the interface between wall–terraces and the crater floor in eastern Hale Crater ($D \sim 125 \times 150$ km; Table 1) shows an excellent example of pitted channelized flows exhibiting several important characteristics related to the presence or absence of pits (Fig. 12; also see HiRISE stereo-derived anaglyph for ESP_020667_1440 and ESP_021511_1440). This image shows a case where a teardrop-shaped streamlined-landform developed when pitted materials behind the lowest tier of terraces in eastern Hale flowed, and was diverted by an isolated terrace blocks while *en route* to the crater floor. Several locations throughout the flow

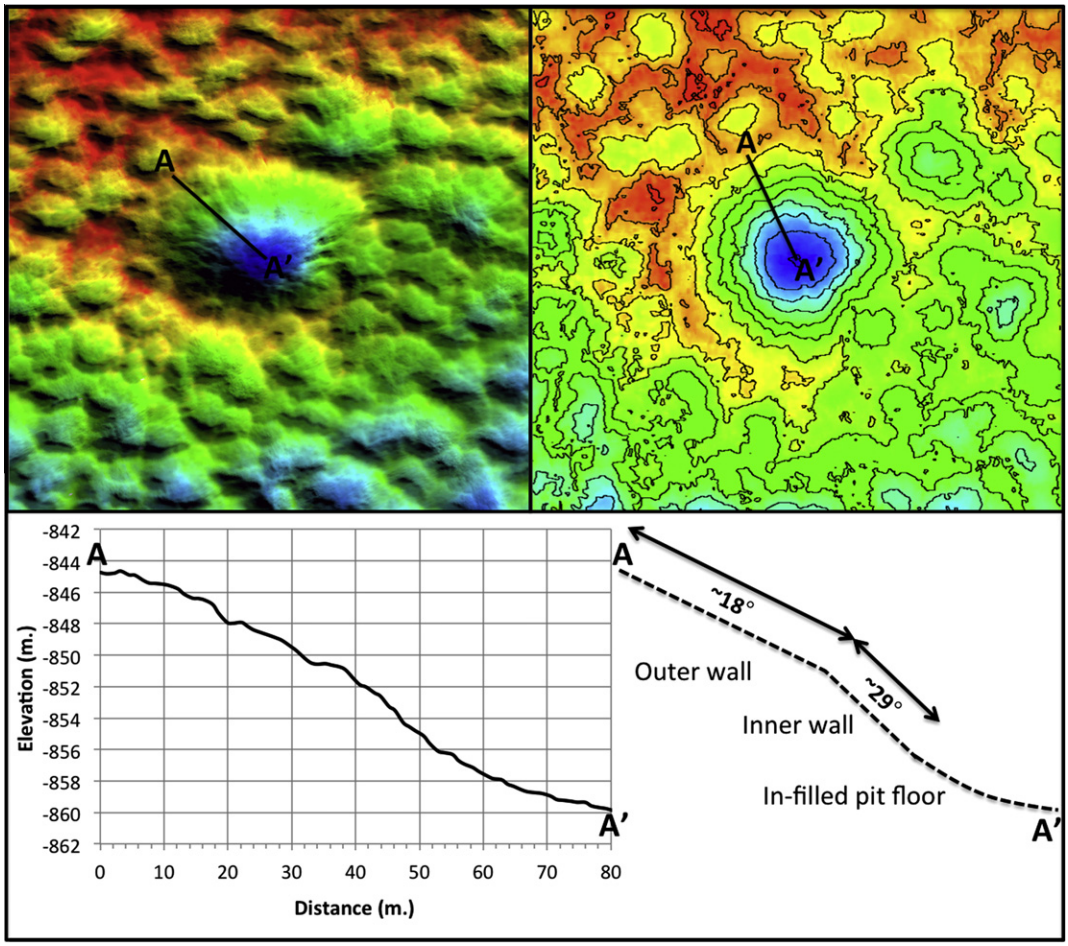

Fig. 5. Morphometric aspects of a relatively large pit (~155 m in diameter) located within the crater-fill deposits of Corinto Crater. (A) A perspective view of a colorized elevation overlain on the orthorectified HiRISE red mosaic, which is then draped on the HiRISE stereo-derived DTM (DTEEC_003611_1970_004244_1970) with a vertical exaggeration set to 3×. (B) A colorized contour map of image (A) with 2-m contour lines. The lowest local elevation is -860 m (on the pit floor) and the highest point locally is −838 m (the "rim" on the NW side of the pit). (C) A NW–SE trending profile into the pit shows that it is ~155 m in diameter and ~15 m deep, and is a good example showing the characteristic 2-slope pit wall described in more detail the text, and observed in other examples where DTMs are available. Image/data credits: NASA/JPL/UA. (For interpretation of the references to colour in this figure legend, the reader is referred to the web version of this article.)

show surfaces with lower pit densities. These include areas where the flow narrowed due to topographic confinement and deposited behind obstacles such as terrace blocks.

Additional observations also indicate a relationship between slope and the presence or absence of pits. Slope measurements of a channelized flow within Mojave's NW wall–terrace region indicate that the slope ranges from ~5–28° over 10 m intervals. Pits are not present on the flows in areas that reach slopes of >15°; pits often reappear along the flow when the slope drops below ~15°.

4.3.3. Ejecta deposits

Discrete ponds of pitted materials conformably overlie the continuous ejecta blanket. These essentially occupy the relatively low topographic areas found in the rugged topography of the ejecta blanket (Fig. 13). The simple crater Zumba (D = 2.8 km; Table. 1; Fig. 14) shows some of the best examples (extending ~0.5–1.5R), which preferentially occur within the eastern and western portions of the ejecta blanket. These ponds are typically observed on lower slopes of the continuous ejecta (~5–10°) following the break in topography between the near-rim ejecta (~20°) and the more distal portions of the continuous ejecta (e.g., Fig. 15). The ejecta ponded and pitted materials also contrast with the surrounding characteristic hummocky ejecta deposits, in that they appear relatively smooth at the scale of CTX and are consistent in tonality. In the case of Zumba Crater, the ponds are notably absent within the northern and southern ejecta deposits. HIRISE observations reveal that the pitted channelized flow features both emanate and connect Zumba's ponded and pitted ejecta deposits to one another (Fig. 13). This is similar to observations of channelized flows within the wall–terrace zone.

Portions of the hummocky ejecta facies appear to be modified and eroded by channel-like features, referred to here as "dissected" (Fig. 13). This dissected ejecta facies is consistently observed to occur only when pitted materials are present. For example, the northern and southern portions of Zumba's ejecta completely lack any sign of this dissected appearance, while the eastern and western pitted material-bearing ejecta exhibit this characteristic dissected appearance. This relationship is also found at other craters; including the smallest simple crater observed with pitted ejecta materials (an unnamed crater in Sinai Planum: "Sinai"; see Table 1). Although it is further degraded than Zumba, a close comparison of the two craters reveals a similar relationship. Hence, the dissected ejecta facies is likely connected to the formation, emplacement and/or modification of the pitted materials.

Transitional and complex crater ejecta exhibit the most extensive pitted materials. Ponds and channelized flows generally occur further out from the main cavity (>0.5R), and even up to and beyond the crater rampart (Fig. 16a). The pitted materials also change

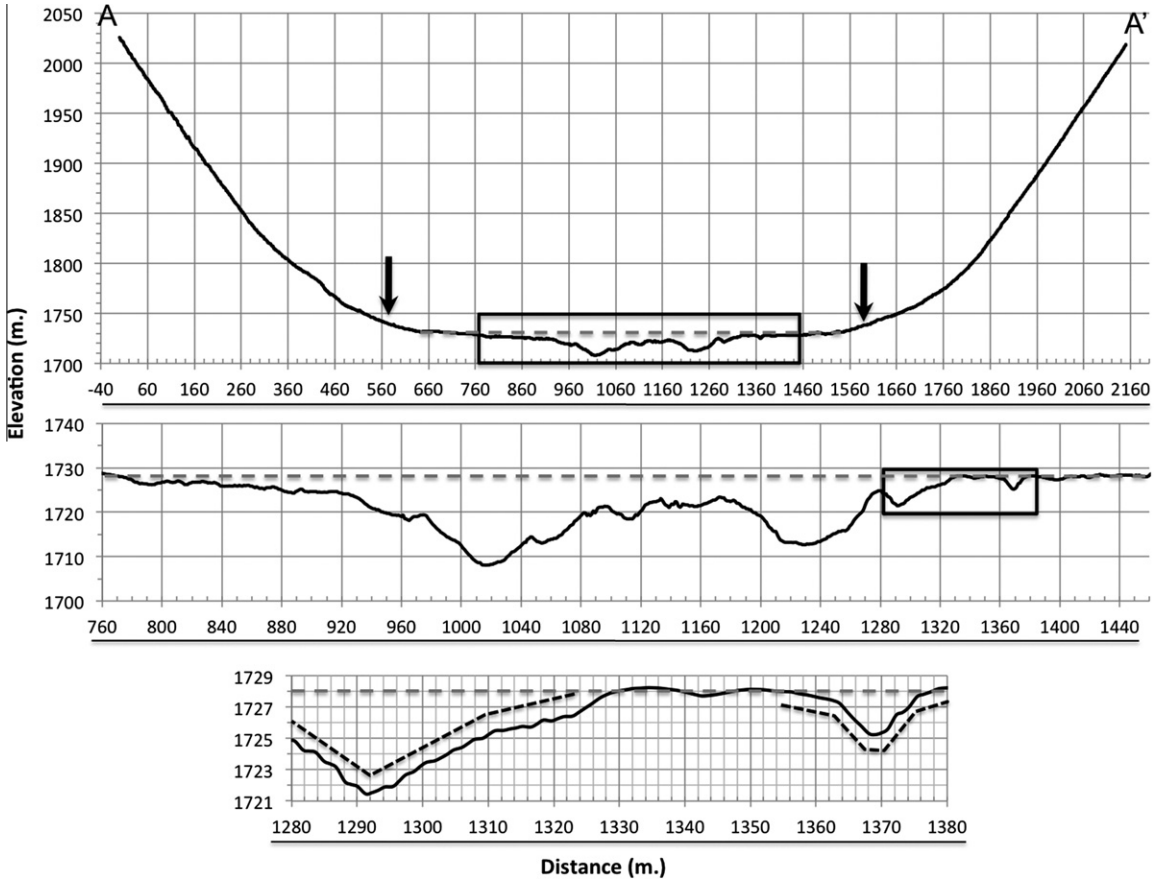

Fig. 6. Zumba Crater elevation profiles (produced from the HiRISE stereo-derived DTM DTEEC_002118_1510_003608_1510_A01). (Top) A WSW–ENE profile of the inner crater walls and crater-fill (vertical exaggeration set to 3×; see A–A′ in Fig. 14 for context). The crater-fill surface generally slopes inward starting at an elevation of ~1732 m and then levels off at an average of ~1728 m (gray dashed-line). The lowest pit floor elevation along this profile is ~1708 m. (Middle) A close-up of the pitted surface of the crater-fill from the profile above. (Bottom) A close-up of two pits showing the general lack of ejecta and obvious raised rim topography that one would expect for secondary or primary craters. The larger pit on the left is the ~50 m-wide, ~5 m-deep pit shown in Fig. 1. The smaller pit is ~28 m-wide and ~3 m-deep. The dashed lines are drawn here to represent the pitted deposit surface and to aid with recognition of the general shape of a pit profile described in Fig. 5 and in the text. Data credits: NASA/JPL/UA.

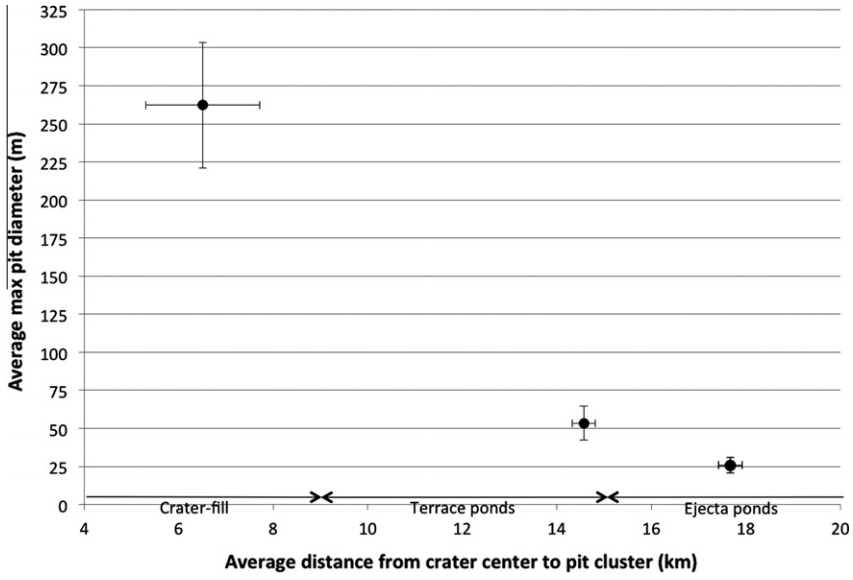

Fig. 7. A plot of the average diameter of the 10 largest pits as a function of distance (i.e., from three basic crater locations: crater-fill, terrace and near-rim ejecta). The general trend is a decrease in average pit-diameter with increasing distance from the crater interior (see text). Error bars are based on statistics and the resolution of the images used for making the measurements.

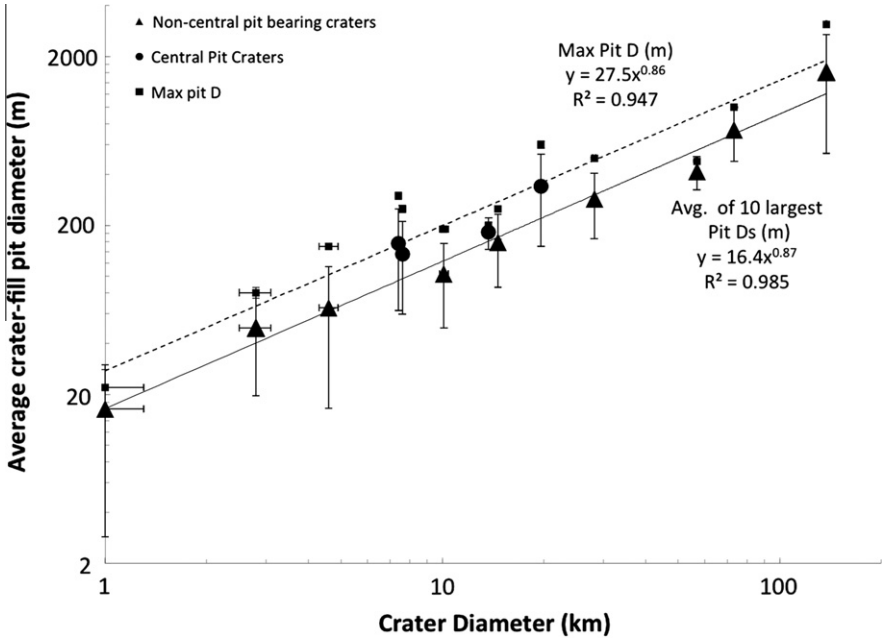

Fig. 8. A plot of the maximum pit diameter (squares) and average of the ~10–12 largest pits (triangles and circles) observed within the crater-fill of 13 pristine or well-preserved craters spanning the entire diameter range of the sample of pitted material-bearing craters presented in this study (D = ~1–150 km). The two pit-diameter trends as a function of host crater diameter are best fit by a power laws. Triangles represent craters with central peaks, while circles represent craters that possess central floor pit structures. Error bars are based on statistics and the resolution of the images used for making the measurements.

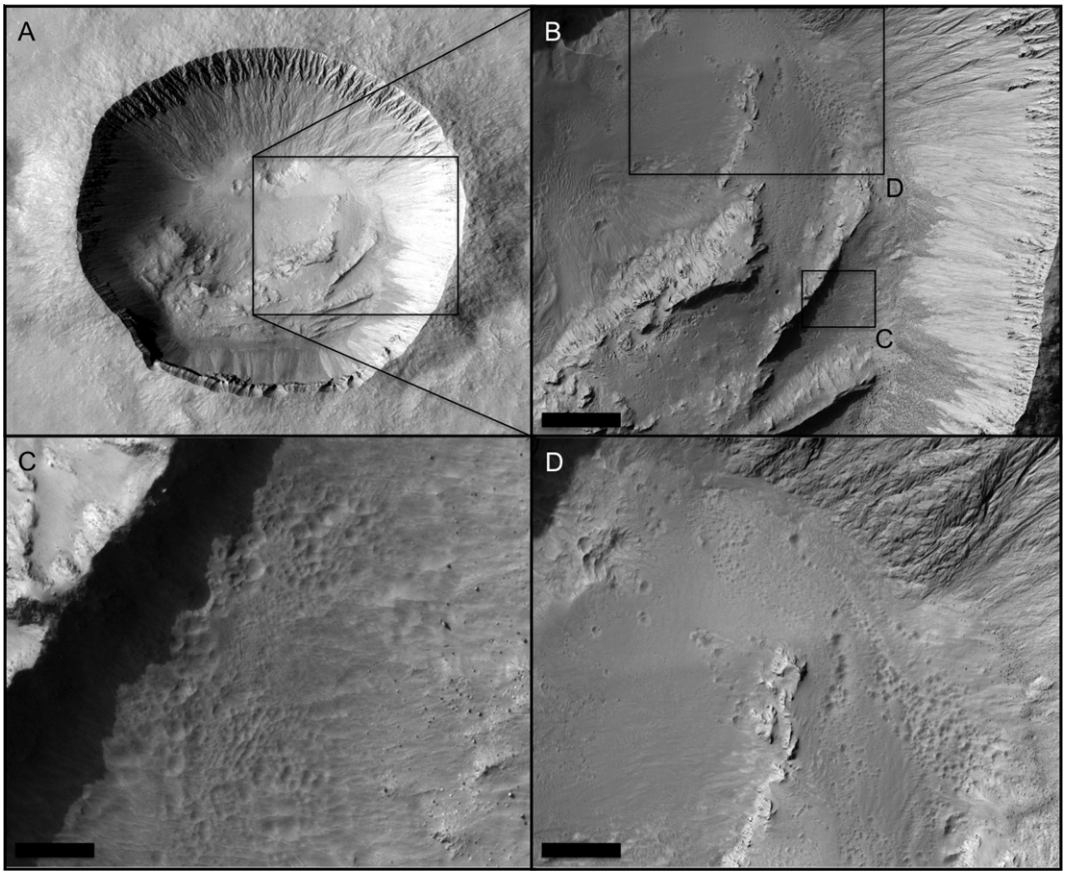

Fig. 9. Images of an unnamed transitional crater (D = 4.6 km) located in Aonia Terra. (A) A CTX subset image (B08_012889_1345) showing two distinct sets of terraces, which likely formed from preexisting structures in the target created by an unnamed ~17.5 km diameter crater to the SE (also, a preexisting graben can be seen trending NW–SE; see CTX image P15_006837_1331). (B) A HiRISE subset image (PSP_006837_1345) of the eastern side of the crater showing ponded pitted materials and pitted flows associated with the terraces. (C) A HiRISE close-up of a pitted terrace pond (D). A HiRISE close-up of a pitted flow that is continuous with the pitted materials on the crater floor. Scale bars: (B) ~250 m; (C) ~60 m; (D) ~130 m. Image credits: NASA/JPL/MSSS and NASA/JPL/UA.

in appearance with increasing crater diameter. In general, the pitted materials of the ejecta blanket become more abundant and interconnected with increasing crater diameter. In transitional complex craters, this initially manifests as a nearly continuous "moat" of ponded and pitted materials that partially or almost completely encircle the primary cavity and where there is a break in slope between the crater rim ejecta and the lower slopes of the continuous ejecta. This is similar to the appearance of the first or highest elevation "tier" of pitted ponds observed in simple craters like Zumba, but in the case of these larger craters, the ponds become more extensive and connected to one another (c.f., Zumba Crater with images of Resen Crater and Noord Crater; see Table 1). Consistent with this observation, both the pitted channelized flows and the discrete ponded and pitted materials become more abundant and less distinct as crater diameter continues to increase. Interestingly, as the pitted ponds and flows become more abundant, they merge and manifest as what appears to be an additional ejecta "layer" (Fig. 16b). This is especially apparent toward the distal end of the ejecta and nearest to the ejecta rampart (c.f., Fig. 16a and b).

5. Discussion

Previously, martian crater-related pitted materials have been suggested to form as a result of impacts into volatile-rich target materials and/or possibly from various crater-related post-impact

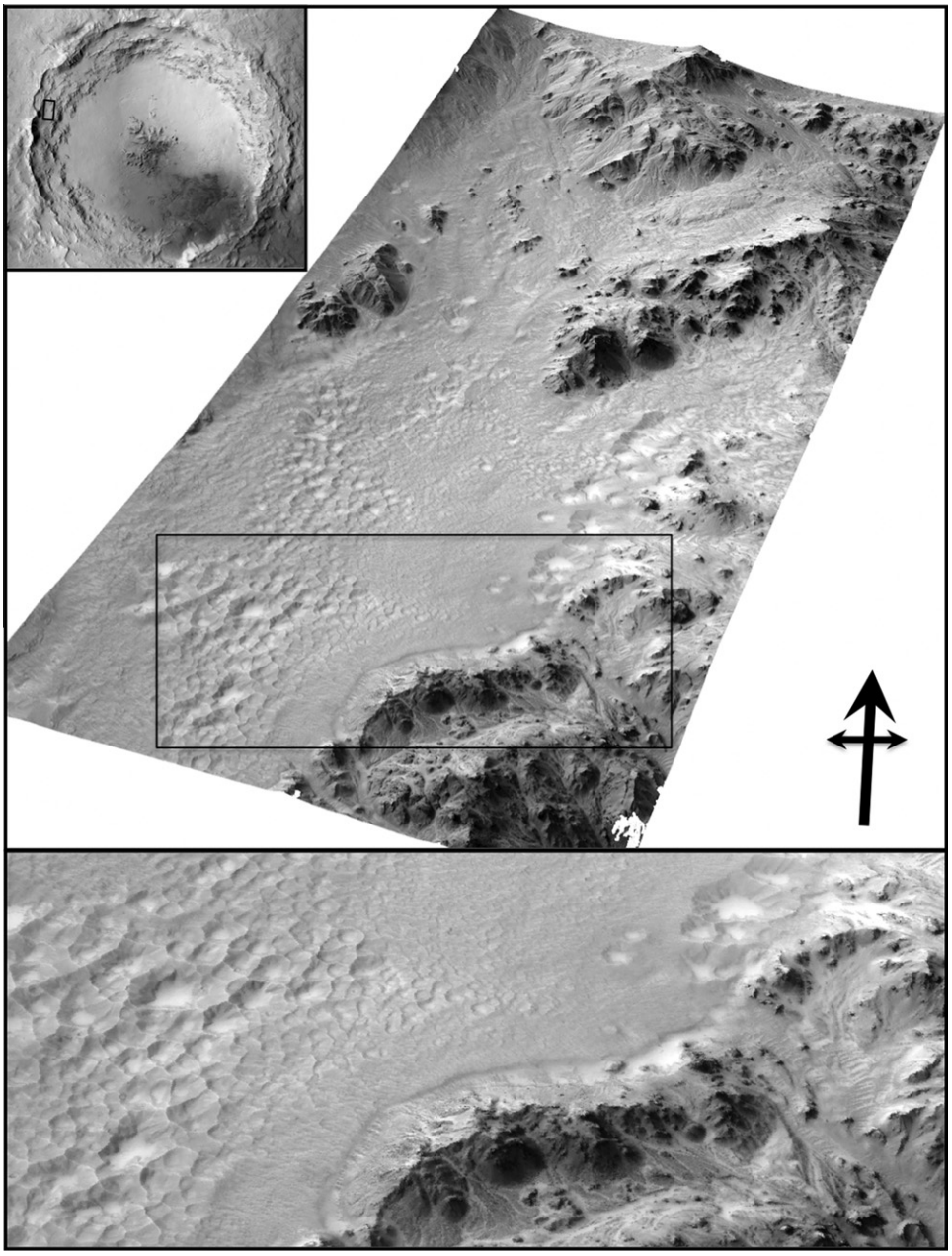

Fig. 10. A 3D northwest looking perspective view of one of Mojave Crater's terraced wall with a CTX mosaic for context (perspective produced from a HiRISE stereo-derived DTM DTEEC_001481_1875_002167_1880_U01 with the vertical exaggeration set to 3×). Ponded and pitted materials are seen here behind a series of terrace blocks located in the NW part of Mojave. "Channelized flows" (Upper right) appear to have been fed by two other ponds found at higher elevations (one to the N and one to the NNE). (Below) This close-up image shows a dense concentration of the pits from the central portion of one of the terrace ponds (Left) as well as a few large pits that appear to have formed at the contact between the pond and the terrace-faulted bedrock (Right). The ponded and pitted materials also show a very distinctive margin with the terrace-faulted bedrock. Note that some light-toned deposits, probably martian dust, sit on the floor of most pits. Image/data credits: NASA/JPL/UA and NASA/JPL/MSSS.

phenomena (McEwen et al., 2007b; Mouginis-Mark and Garbiel, 2007; Tornabene et al., 2007a, 2007b; Morris et al., 2010; Hartmann et al., 2010). Note that when referring to the volatile-rich nature of the pre-impact target, we are referring specifically to water and/or water–ice, but min the case of Mars this may include other undetermined volatile species (e.g., CO_2). Table 4 presents a summary of both previous and newly observed characteristics, which along with the more detailed discussion in the next section; provide support for an impact origin for the crater-related pitted materials.

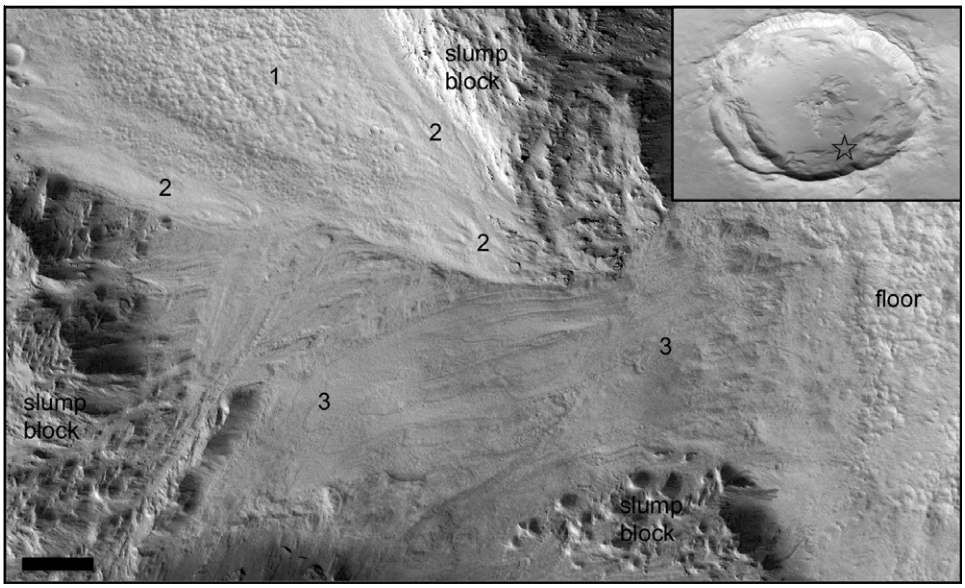

Fig. 11. A HiRISE red mosaic image (PSP_005771_2035) that covers a portion of a pitted flow found within the western wall slumps of Tooting Crater (Upper left – an oblique CTX image of Tooting for context – B17_016412_2036). A series of flows are observed to originate from ponded and pitted materials deposited behind slumped terrace blocks at higher elevations (not shown; see above CTX image in full). (Upper left) A non-pitted, possibly 2nd generation flow, superposes the first pitted flow. These flows are continuous with the pitted deposits on the crater floor (Right). What appears to be a 3rd generation flow – consisting of relatively thin, pit-free, overlapping multiple flow layers – superposes both flows 1 and 2. These multi-generational flows are also observed at other craters (see HiRISE images of the interior of Zunil Crater). Note that the later stage flow appears to superpose pitted materials on the crater floor. Scale bar: ~120 m. Image credits: NASA/JPL/UA and NASA/JPL/MSSS.

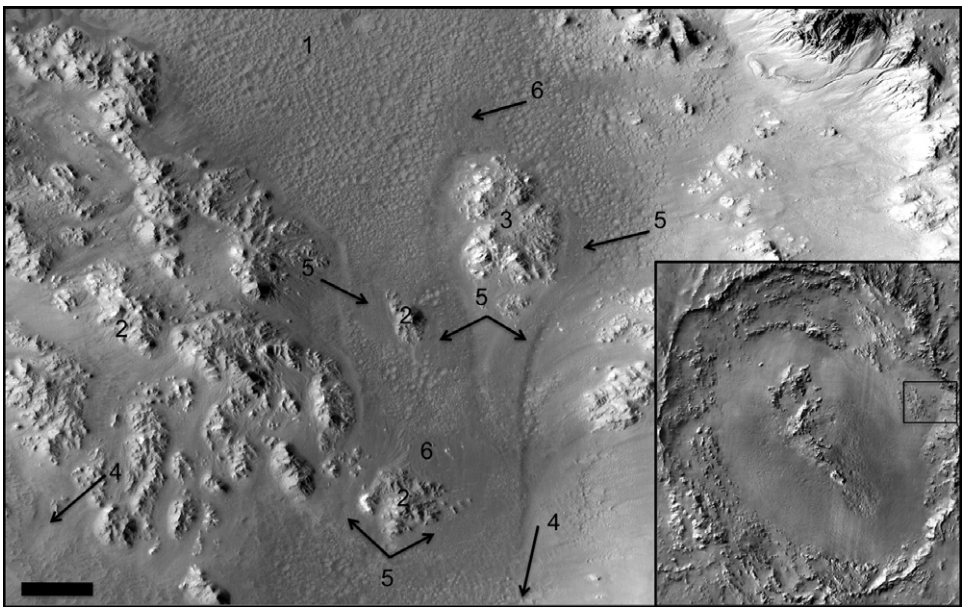

Fig. 12. CTX image (P05_002932_1445) of pitted materials associated with the terraces and crater floor of Hale Crater located on the northern portion of Argyre Basin. This example further highlights the complex relationships of the "pond" and "flow" morphologies. Ponded and pitted materials are either confined as a deposit, or pond (e.g., 1), or diverted as flows by obstructing terraces blocks (2). One particular pond at (1) appears to be the source of a series of flows, which formed a teardrop-shaped streamlined landform further down slope at (3). The flow appears to have continued down slope and was diverted by additional isolated terrace blocks while *en route* to the pitted deposits on the crater floor (4). Several locations throughout the flow do not show densely pitted surfaces (5), which include areas where the flow narrowed due to confining obstacles, but also includes areas behind smaller obstacles (6). Scale bar: ~1.7 km. (Bottom right) A THEMIS daytime brightness temperature mosaic of Hale for context. Note that crater-fill pits (densely clustered around the central peak) are resolved in this 100 m/pixel THEMIS mosaic. Image credits: NASA/JPL/MSSS and NASA/JPL/ASU.

5.1. An impact origin for crater-related pitted materials

The results of this study are consistent with crater-related pitted materials being primary impact-formed deposits. A key observation supporting an impact origin is that their distribution is similar to the distribution of impact melt-bearing deposits within and around lunar, mercurian, and terrestrial craters (e.g., Hawke and Head, 1977; Osinski et al., 2011). In general, the majority of the highly shocked and melt-rich materials preferentially remain in the original transient crater (e.g., Grieve et al., 1977), but volumes of these materials scale disproportionately with increasing transient cavity diameter (e.g., Cintala and Grieve, 1998). Consequently, as crater diameter increases, additional highly shocked and melt-rich deposits are emplaced both within and outside of the final crater, which is consistent with theoretical, numerical (Grieve and Cintala, 1992; Cintala and Grieve, 1998) and empirical observations (Hawke and Head, 1977; Cintala and Grieve, 1998; Bray et al., 2010; Osinski et al., 2011).

After their initial emplacement, hot, melt-rich impact deposits are often subject to additional movements due to gravitational effects, crater modification, and continued flow after modification due to topography of both the pre-existing target and the final crater (Hawke and Head, 1977; Cintala and Grieve, 1998; Bray et al., 2010; Osinski et al., 2011). This may explain why ponds appear to be sources for flows and how multiple pit-bearing flows are observed to superimpose one another. This is also consistent with the examples of crater modification and pre-impact topography possibly influencing the location of the pitted materials in transitional and complex craters reported herein (e.g., Resen, "Ascraeus" and the unnamed crater in Valles Marineris). Osinski et al. (2011) discuss the origin and emplacement of impact melt and ejecta deposits around craters on the terrestrial planets in detail. Impact melt-bearing deposits can be found on crater floors, terraced rim regions, and in the ejecta deposits—corresponding to the location of pitted materials in martian craters. Furthermore, pitted materials superpose the deposits of the continuous ejecta blanket, which is consistent with impact melt-rich deposits and is explained by Osinski et al. (2011) via a multi-stage impact ejecta emplacement model.

In addition to the above considerations, it is difficult to explain pit size as a function of post-impact deposition because the scale of such deposition would have to be nearly global and uniform over a large expanse of martian geologic time. Similarly, the correlation between pond size and the size of the host crater is crucial. With respect to an impact origin hypothesis for the pit-bearing host materials, this pond-to-crater size relationship may generally reflect the expected volume-to-diameter scaling behavior of the volume of hot deposits, including both shocked and impact melt-bearing materials to the crater's diameter (Grieve and Cintala, 1992; Cintala and Grieve, 1998; Pope et al., 2006). Observation of pitted materials that do not occupy the entire crater-fill of the smallest simple craters in our sample is consistent with this hypothesis, as smaller craters generate exponentially lower melt volumes than larger craters. Furthermore, observations of an increase in extent of crater ejecta pitted materials with increasing crater size are also consistent with an impact hypothesis.

Moreover, the occurrence of outcrops containing meter- to decameter-sized light-toned rounded to angular rock fragments

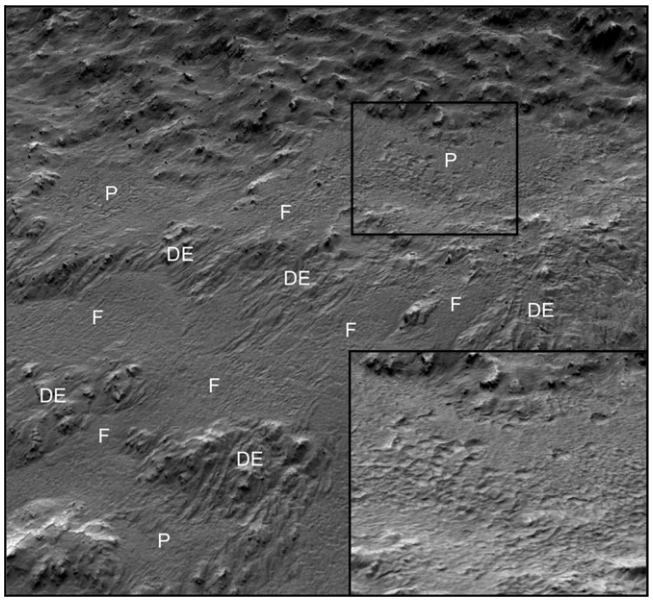

Fig. 13. A 3D west-looking perspective view of the pitted materials associated with the eastern ejecta blanket of Zumba Crater (perspective produced from a HiRISE stereo-derived DTM DTEEC_002118_1510_003608_1510_A01 with the vertical exaggeration set to 3×). Hummocky ejecta deposits are seen here rising up to the crater rim in the background. Pitted materials lie ~625 m (~0.45 crater radii) from the crater rim, and form a discontinuous unit that both overlies and embays discrete "patches" of the blockier more rugged hummocky ejecta facies. These patches of the hummocky ejecta appear to be cross-cut by channel-like features (referred to here as "dissected" hummocky ejecta – DE). DE patches are absent from the uppermost portion of the hummocky ejecta seen here, but also throughout the northern and southern ejecta of Zumba Crater where pitted materials are completely absent (see Fig. 14). These observations are consistent with other pitted material-bearing craters, including larger complex craters (e.g., Zunil Crater). (Bottom right) A close-up of pitted materials with a relatively level surface, and that appears to be encapsulated in a topographic low within the ejecta (i.e., a "pond" – P). "Channelized flows" (F) appear as relatively smooth and often pitted materials with slopes ranging from ~5° to 10°. Flows appear to be sourced from higher topographic ponds and appear to connect with ponds that are further down-slope. The flows are generally narrower then the ponded and pitted materials and sometimes possess pits that are generally smaller than the pits associated with the ponds. Pits in both Zumba's ponds and flows are generally ~5–20 m in size with the ~20 m pit being the largest observable ejecta pit size. These general observations from the eastern ejecta are consistent with ponds and flows on the western ejecta, which occur within ~535 m (~0.38 crater radii) from the crater rim.

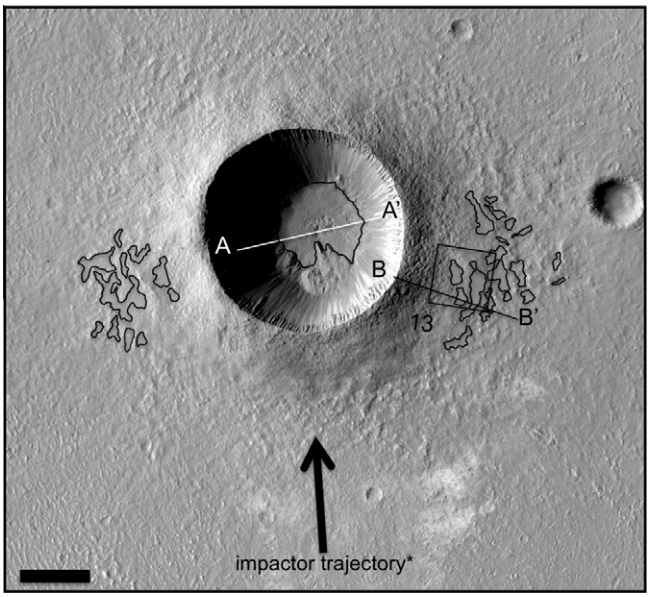

Fig. 14. A CTX context image (P05_002830_1511) of Zumba Crater. The largest crater-fill pits can be just discerned in this context image (c.f., Fig. 1). Although the aspect of this crater is mostly symmetrical, Zumba Crater possesses a distinctive asymmetric "thermal" ray pattern (see THEMIS TIR observations of Zumba or Fig. 4 in Tornabene et al. (2006)). This suggests Zumba formed from a moderately oblique impact from the SSE. Like the unnamed crater in Sinai Planum (see Table 1), Zumba's pitted deposits are notably absent on the northern and southern portions of its ejecta blanket, and are only observed in the ejecta deposits that are approximately perpendicular to the inferred impactor trajectory. Scale bar: ~1 km. Image credit: NASA/JPL/MSSS.

associated with the pit walls also supports an impact origin. Based on their appearance, geologic setting and the preservation of their host craters, these are best explained as impact melt-rich breccias, which are commonly observed both interior and exterior to terrestrial impact structures (Stöffler and Grieve, 2007).

Finally, we note that in studies of impact melts on the Moon, craters that are considered to be the "youngest", are typically sought to observe unmodified impact melt-bearing crater-fill and ejecta deposits (e.g., Hawke and Head, 1977; Bray et al., 2010). Given the additional active geologic processes Mars possesses when compared to the Earth's Moon, craters that show relatively unmodified impact-melt bearing deposits should represent a subset of the crater population on Mars. A "young" crater population should be randomly distributed across the martian surface, and approximately equal in both the northern and southern hemispheres; this is consistent with the results of our survey.

5.2. Nature of the pitted materials

Despite some similar gross morphologic characteristics between pristine lunar and martian crater deposits (e.g., ponds and flows), an obvious distinction between the two is the presence of numerous and densely clustered pits in martian craters. The latest high-resolution images of lunar impact melt-bearing deposits, particularly the crater-fill, reveal characteristically hummocky and smooth, pit-free deposits (e.g., Bray et al., 2010). Interestingly, only nine pristine and well-preserved craters with lunar-like primary deposits have been identified on Mars thus far. One of the best examples on Mars is Pangboche Crater (D = 10.3 km; Table 1). Pangboche is located within the sparsely cratered, and what is likely a basaltic target (e.g., Lang et al., 2009), high atop Olympus Mons (~21 km elevation). Despite significant cover by martian dust, this crater compares very well with the lunar, rayed crater Moore F (Fig. 17). Given that the martian crater-related pitted materials are primary (i.e., linked to crater formation), the lack of pitted crater-fill deposits on the Moon yields an important clue with respect to the origin of the pits on Mars.

The upper crust of the Moon and Mars as an impact target are very distinct with respect to volatile contents, which has been a key aspect discussed in numerous papers on the origin of layered ejecta blankets on Mars (see Barlow (2005) and references therein). The upper lunar crust is a notably volatile-poor target, while the majority of upper crust of Mars, based on theoretical and empirical evidence, is volatile-rich (see review by Carr (2006)); therefore, one possible suggestion is that the pits form as a consequence of some secondary mechanism from impacts into volatile-rich target materials. Subsurface volatiles on Mars, believed to be predominately water and water–ice, manifests as a kilometers-thick global cryosphere and hydrosphere, which vary in depth both as a function of topography (crustal thickness) and latitude (Clifford, 1993; Clifford et al., 2010; Mellon and Jakosky, 1995; Mellon et al., 1997). During a hypervelocity impact event into such a target, both ice and silicates are brecciated and melted to form volatile-rich impact melt-bearing deposits. In addition to possibly explaining the pits, these volatile-rich impact melt-bearing deposits may also be responsible for other observed features such as fluvial features described in a series of recent studies of the craters Mojave, Hale and Lyot (Williams and Malin, 2008; Harrison et al.,

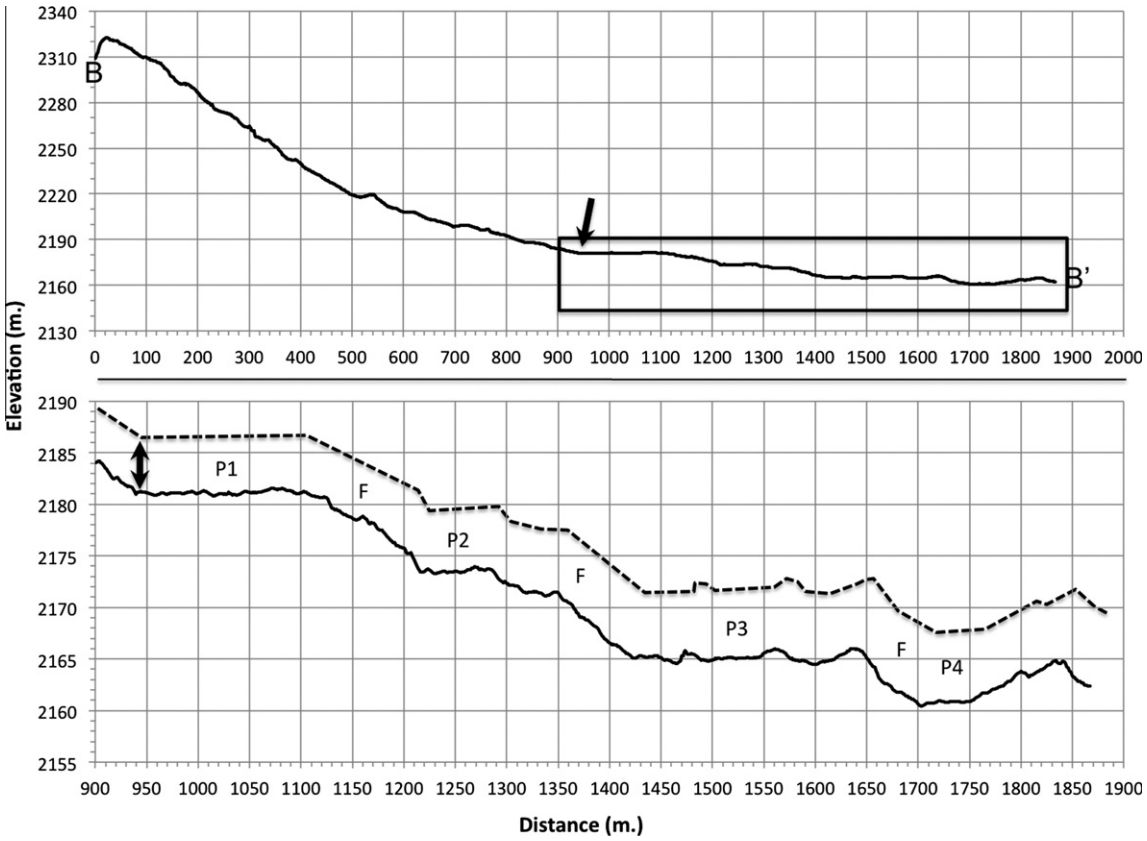

Fig. 15. Zumba crater ejecta profiles taken from the DTM DTEEC_002118_1510_003608_1510_A01 (see B–B' in Fig. 14 for context). This profile highlights four distinct topographic tiers of ponds (P) and associated flows (F). (Top) The profile shown here extends ~1.3R from the crater rim and has a vertical exaggeration (VE) of 3×. The average slope starting from the rim ~20°, which then drops to less than 5° from at a discrete break in topography at ~0.6 R from the rim (black arrows). (Bottom) This is close-up of the pond- and flow-bearing portion of Zumba's ejecta with a VE of 10×. The relatively flat (very low slopes <3°) portions correlate with ponds in both planview and perspective views from HiRISE and CTX (c.f., Figs. 13 and 14), while the relatively steeper areas between the ponds (~5–10°) correspond to the flows in the image.

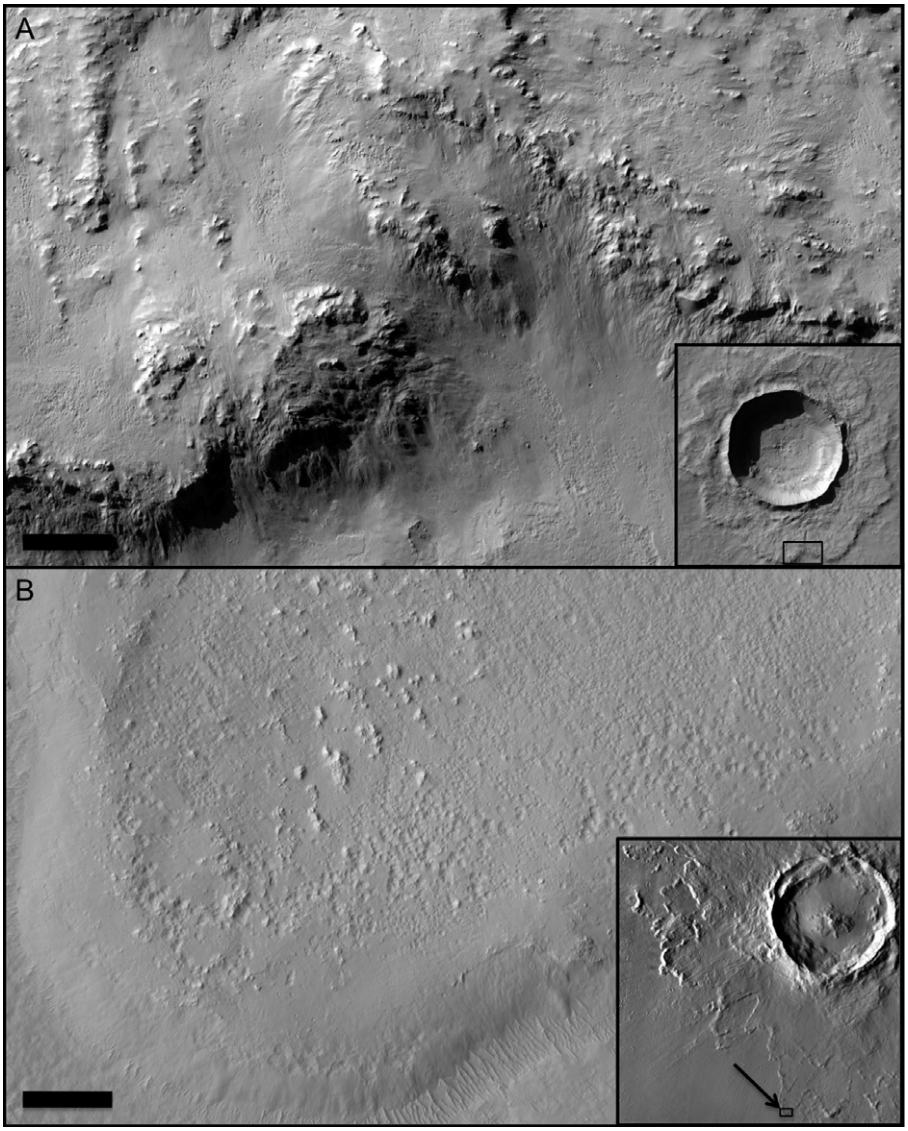

Fig. 16. HiRISE close-ups of distal ejecta pits observed at a transitional crater (Resen Crater) and a complex crater (Tooting Crater). (A) A close-up of Resen Crater's (PSP_008135_1520) continuous ejecta exhibiting extensive pitted materials (both pond and flow types). (B) A close-up of a Tooting Crater's (PSP_009832_2030) ejecta pits, which appear to occur directly into the surface of the continuous, and in some cases, the discontinuous ejecta just beyond the crater rampart. Scale bars: (A) ~180 m; (B) ~250 m. Image credits: NASA/JPL/UA and NASA/JPL/ASU.

2010; Jones et al., 2011), but also the dissected appearance of crater ejecta when it is closely associated with ejecta pitted materials (e.g., Fig. 13).

Like Mars, Earth possesses volatile-rich target materials. So, if impacts into a volatile-rich silicate target are responsible for forming pits, or at least something analogous to them, should they not also form in terrestrial craters? Laboratory analyses of melt-bearing breccias from the Ries impact structure in Germany, confirm a high volatile content for some of its impactites (hydrated glasses with up to ~20% by weight H_2O; Osinski, 2003). In addition, field studies of eroded outcrops of impact melt breccia deposits indicate the presence of abundant vertical vent structures, which are described as "degassing pipes" or "vertical steam channels" by Newsom et al. (1986) possibly analogous to the martian crater-related pits in cross-section. These degassing pipes were noted to increase in number and density stratigraphically up section. These pipes may be analogous to the martian pits in cross-section. Unfortunately, the extent of terrestrial erosion and modification prevents a direct overhead view of these terrestrial impact structure features for a direct comparison with the martian pits.

The results from this survey indicate that the sample population of pitted material-bearing craters has a slight preference for layered ejecta morphologies and central floor pits (Table 2). The proposed origin of these morphologies (see review by Barlow and Bradley, 1990), if correct, lend further support that target volatiles may play a role during the formation of pits. However, approximately 13% of all pitted-material-bearing craters in our sample population possess radial ejecta, which has been interpreted to represent impacts into relatively volatile-poor target materials (e.g., Barlow, 2005). Yet, it is important to note that the impact sampling depth for ballistic ejecta is shallower when compared to the sampling depth of the materials from which the melt is derived (Osinski et al., 2011). This suggests that if target volatiles are responsible for crater-related pitted materials, then radial ejecta-bearing craters may represent impacts into targets that are relatively volatile-poor within the upper excavation zone and

Table 4
Summary of observations and supporting evidence for an impact origin for the crater-related pitted deposits.

Attributes	Interpretation	Figures
Are consistently superimposed by debris flows, talus and mass wasting features associated with crater modification and post-impact processes	Indicates that the pitted materials are crater-formed deposits, or that they formed not too long after the crater-forming event	Figs. 1, 9, 11 and 12
Observed primarily as ponded and flow materials located in three specific areas – crater-fill, terraces and ejecta (ejecta distribution shows a relationship to the inferred impact trajectory of the host crater)	Consistent with the distribution of non-ambient impactites including impact melt-rich deposits; inconsistent with a post-impact deposition	Figs. 1, 4, 9–14 and 16
Occur within the most pristine and best-preserved craters as exemplified by young crater retention ages and high d/D properties; Crater degradation correlates with pit degradation. The 196 craters identified in this study are almost divided equally between the northern and southern hemispheres	Consistent with an impact origin, but also consistent with deposition that potentially followed post-impact (e.g., lacustrine deposition); Distribution is consistent with a unbiased crater population, which may reflect a preference for fresher craters	Figs. 2 and 3
Pits are primarily confined to ponded and flow features, which superimpose or embay crater displaced bedrock and ejecta. Pits have not been observed that cross-cut a geologic boundary (i.e., between the pitted materials and ejecta or displaced bedrock)	Same as above; but also inconsistent with the interpretation of pits as overprinting secondary or primary craters	Figs. 1, 9, 11 and 12
Light-toned fragments (possible breccias) are observed to outcrop in non-dusty and well-exposed pit walls	Similar to terrestrial crater-fill breccias and consistent with an impact deposition interpretation	Fig. 4
Pit size scales with crater diameter, and the size (or area) or the pitted unit in an individual crater	Consistent with pit formation having ties to formation of highly shocked non-ambient deposits (i.e., function of heat generated and volume of volatiles present in target materials)	Figs. 7 and 8
Various morphologic and morphometric evidence of pitted materials exhibiting fluid mobility during emplacement such as flow morphology with respect to obstacles, "ponds" with quasi-equipotential surfaces and the connectivity of ponds and flows with the deposits of the crater-fill	Consistent with an impactite flow origin; inconsistent with post-impact deposition	Figs. 9–14 and 16
Ejecta blanket pitted materials appears to scale up, become more areally extensive and morphologically complex with increasing crater diameter	Consistent with an impact origin & may reflect the disproportionate increase in impact melt volume with respect to crater size (see Refs. in text); inconsistent with post-impact deposition	Figs. 13, 14 and 16

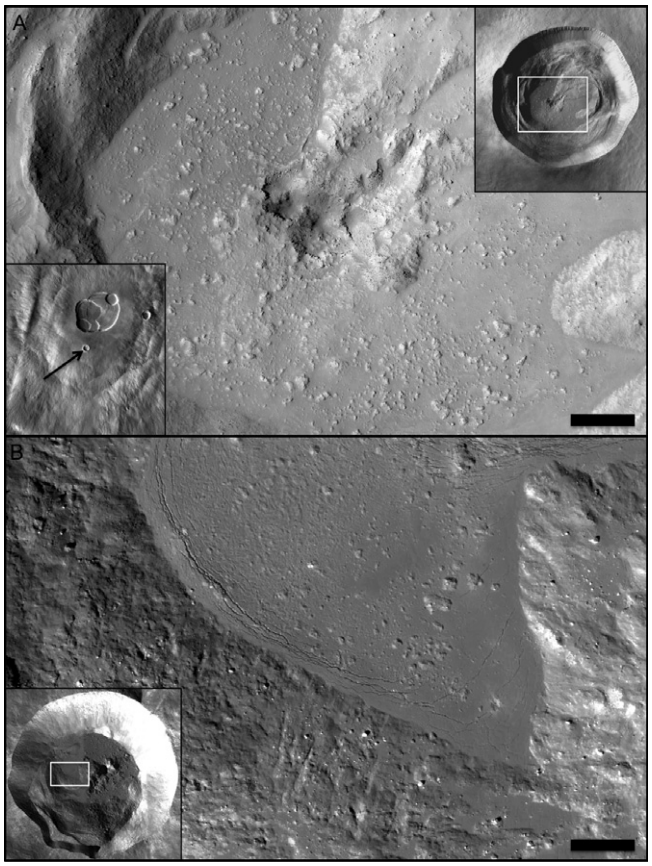

Fig. 17. Examples of smooth and hummocky quasi-equipotential crater-fill deposits in both martian and lunar craters, generally interpreted to be volatile-poor melt-rich crater-fill deposits. (A) A close-up of the crater-fill of the fresh martian crater Pangboche (HiRISE image: PSP_001643_1975 and CTX context image: P02_001643_1974) located high atop (~21 km elevation) Olympus Mons. (B) A close-up of the crater-fill of the fresh lunar crater Moore F (D = 24 km; 175.0°E, 37.4°N) from the LROC NAC image (M105664582RC; ~1.66 m/pixel; WAC context mosaic with superimposed NAC images courtesy of JMARS for the Moon). Scale bars: (A) ~500 m. (B) ~500 m. Image credits: NASA/JPL/UA, NASA/JPL/MSSS, NASA/JPL/ASU and NASA/GSFC/ASU.

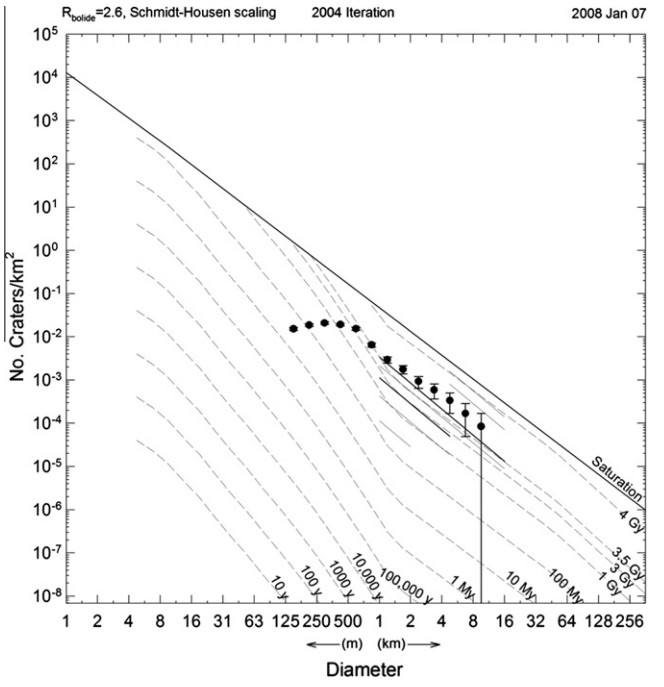

Fig. 18. A Hartman-style log–log incremental plot with isocrons (see Hartmann, 2005) showing the size–frequency distribution of overprinting craters associated with the pitted crater-fill deposits of Bakhuysen crater (D = ~150 km; 344.3°E, 23.2°S). Approximately 1200 superimposed craters were counted over an area of ~11820 km^2.

more volatile-rich at greater depth. If this is correct, then such craters may be useful to determine the possible depth of this interface. Furthermore, the presence of both volatile-poor and -rich melt-bearing materials within a single crater is not uncommon in terrestrial examples into mixed targets that include volatile-rich and volatile-poor rocks (Newsom et al., 1986; Grieve, 1988; Jones et al., 2000; Osinski, 2004). This may be exemplified by crater fill

deposits of Tooting Crater, which possesses a relatively pit-poor and fractured lunar-like material in the southern portion of its crater-fill deposits, and densely pitted materials within the Northern portion of the crater-fill (see Fig. 6 in Mouginis-Mark and Garbiel (2007)). As such, the relatively pit-poor materials in Tooting's southern crater-fill may represent impact melts that are volatile-poor; whereas the pitted materials in Tooting's northern crater-fill may be analogous to volatile-rich impact melt-bearing breccia deposits.

Our survey of pitted material-bearing craters on Mars indicates a lower frequency of these craters within equatorial regions, at high latitudes, at extreme elevations, and in certain regions (e.g., Arabia Terra, Utopia Planitia and Hellas Basin). The equatorial restriction is consistent with our hypothesis, particularly as it pertains to the general variations of target volatiles with respect to latitude and elevation. Further work is needed to test the hypothesis that the expected desiccation of equatorial regions (Clifford et al., 2010) leads to fewer equatorial craters with pitted deposits. Arabia Terra is known for its complex history of burial and exhumation (Malin and Edgett, 2001; Edgett, 2005). As such, the preservation of crater-related pitted materials in this particular region may be particularly low. However, it is important to note that there may also be an MRO observational bias with relatively less HiRISE and CTX coverage of Arabia Terra when compared to other dusty areas on Mars. Moreover, there are likely complications at high latitudes and low elevations with respect to preservation (e.g., Utopia Planitia and Hellas Basin). Such regions on Mars are subject to active seasonal, periglacial, and polar processes (Squyres et al., 1992; Banks et al., 2010), which rapidly overprint original crater morphologies on the order of $\sim 10^5$ years (Korteniemi and Kreslavsky, 2011). If crater-related pitted materials represent primary crater deposits, then the high geologic activity of these regions could be responsible for the paucity to complete lack of pitted material-bearing craters in Utopia Planitia and Hellas Basin, respectively.

Furthermore, we speculate that pit formation in impact deposits may require a critical water/ice–silicate ratio in the target materials, which may also be reflected in the distribution of pitted material-bearing craters on Mars. The observed pit diameter dependence with respect to crater diameter and radial distance from the center of the crater may reflect that heat and volatile concentrations could be contributing factors to the number and size of the pits formed. Nonetheless, an outstanding question remains as to why pitted materials are typically not observed in craters poleward of $\sim 60^\circ$, where one would expect higher concentrations of near-surface H_2O. One possibility is that extremely volatile-rich target materials may lack sufficient cohesive materials to form pits (e.g., high-latitudes and very low elevations). The lack of these pitted materials in pristine craters on icy satellites, where water/ice–silicate ratios are very high, is consistent with this hypothesis, although we note here that the image resolution for these bodies may be insufficient to resolve these features. This may also be reflected in a lack of pitted materials in DLE craters (Table 2), which are suggested to form target materials with high concentrations of shallow subsurface ice (Boyce and Mouginis-Mark, 2006), may also reflect a relationship between pits and a critical water/ice–silicate ratio. However, we also note that this may be a function of DLE abundance and preservation, or a consequence of the fact that many DLEs are preferentially found >35°N or S latitude where crater-related pitted materials occur less frequently (Fig. 2); DLEs also appear to have a target type preference (Barlow and Perez, 2003), while pitted material-bearing craters do not. One possible idea to test this hypothesis would be to look for a relationship where the number of pits in the crater-fill deposits normalized to crater size (or crater-fill area) would vary as a function of latitude.

5.3. Pit formation mechanism(s)

Various kilometer-scale pits, cavities or depressions have been reported on Mars (e.g., Burr et al., 2009). These landforms generally form by the removal and/or displacement of some volume of materials. For Mars, these include (1) numerous pristine and degraded impact craters (Craddock et al., 1997; Bleacher et al., 2003; Garvin et al., 2003; Boyce et al., 2006), (2) craters produced by primary phreatic and phreatomagmatic explosions (Morris and Mouginis-Mark, 2006; Fagents and Thordarson, 2007; Jaeger et al., 2007; Burr et al., 2009), (3) cratered cone groups and thermokarst terrains produced by interactions between lava flows and near-surface water and/or ice (Keszthelyi et al., 2008; Burr et al., 2009; Hamilton et al., 2010c, 2011), (4) devolatilization of pyroclastic density currents (Ghent et al., 2012), (5) collapse pits associated with tectonic structures or drainage of lava lakes/tubes (i.e., pit craters; Okubo and Martel, 1998; Wyrick and Ferrill, 2004; Rowland et al., 2011), (6) mud volcanism (Burr et al., 2009; Skinner and Tanaka, 2007), (7) various ablation and/or sublimation features related to ice-rich terrains, ice-cored mounds, or ice blocks (Lucchitta, 1981; Mustard et al., 2001; Pierce and Crown, 2003; Soare et al., 2007, 2008; Kadish et al., 2008; Searls et al., 2008; Burr et al., 2009; Hartmann et al., 2010), and (8) some complex aeolian structures, such as ergs that can develop negative relief features between a high-standing network of star dunes (Edgett and Blumberg, 1994; Bridges et al., 2007; Bourke et al., 2010). Pits or pit-like features formed in each these settings have distinctive morphologic and geologic characteristics and are often confined to a specific geologic setting, such as a volcanic province. The pitted materials described in this study are exclusively associated with an impact crater facies. As such, the pits and their host materials must be related to the impact cratering process or be unique to post-impact environments.

Although the crater-related pits share some morphological similarities with the features listed above, none of their characteristics are entirely consistent with the pitted-materials, nor are any of these other landforms exclusively associated with impact structures. Among the alternatives, impact-related pitted material exhibits the greatest morphological and geospatial similarities to dense populations of craters formed during explosive lava–water interactions (e.g., Hamilton et al., 2010a, 2010b) and crater groups formed within hot debris flows that have interacted with near surface water (e.g., Moyer and Swanson, 1987). Crater-related pitted materials are morphological similar to secondary explosion craters formed by rapid escape of heated volatiles, but their mechanisms are likely to be fundamentally different in that volatile sources would be different. If the host materials for the martian crater-related pits are equivalent to terrestrial suevite deposits (i.e., impact melt-bearing deposits), then the volatiles would be primarily located within the hot deposit, but could also come from its surroundings (i.e., low shock target rocks). In this sense, the formation mechanism may be more similar to degassing of volatiles entrained within hot pyroclastic density currents, as proposed for the formation of small cones within Isidis Plantia by Ghent et al. (2012), with morphological differences largely related to the nature of the host material, abundance of entrained water, and energetics of the degassing processes.

Based on these comparisons, and the likelihood that the host deposits were emplaced as hot impact melt-bearing deposits that may have entrained volatiles from volatile-bearing target materials, Boyce et al. (2011, 2012a, 2012b, submitted) suggest that these pits are the morphologic expression of degassing pipes and their associated vents. Water entrained within the ejecta deposits would rapidly vaporize and begin to escape. As the bubbles coalesced they would form streams of gas that transport volatiles and particles towards the surface. The escaping gas–particulate mixture would

erode the conduit walls and expand the vents to produce a network of pits within the impact deposits. Erupted particles may have formed fall deposits that drape the host material, but their topographic expression is subtle and do not appear to have generated constructional features that stand above the local datum. Once the impact deposits are thoroughly degassed, conduit walls may have collapsed to produce the final pit morphology. At depth, these conduits may be similar to the gas escape pipes observed by Newsom et al. (1986) at the Ries impact structure. The specifics of the pit-forming process are outside the scope of this study, but are addressed in detail by Boyce et al. (2012b, submitted).*5.4. How long have crater-related pitted materials been forming on Mars?*

The largest pitted material-bearing crater in our database is Bakhuysen Crater ($D \sim 150$ km). Here we use crater-counting statistics collected from within its crater-fill deposits, with the idea that Bakhuysen may represent one of the oldest craters in our global database. Preserved pitted materials, also including polygonally fractured surfaces like those seen in Tooting Crater, are recognized in northern and northeastern sections of Bakhuysen (see CTX image listed in Table A.1). A log-incremental plot of the SFD of overprinting impacts (Fig. 18), along with isochrons (Hartmann 2004 iteration; see Hartmann, 2005) and the major time-period boundaries for Mars, indicate a modeled crater-retention age that is consistent with late Noachian or Noachian–Hesperian time. These results suggest that crater-related pitted materials have been forming in craters throughout much of martian geologic history. If our hypothesis is correct, target volatile contents of the martian crust played a role during the impact process since the Noachian. This is consistent with the suggestion that crustal volatile contents have not varied significantly since that time (Barlow, 2004).

6. Conclusions

Crater-related pitted materials were once recognized in only just a few examples of the most pristine craters on Mars (Mouginis-Mark and Garbiel, 2007; Preblich et al., 2007; Tornabene et al., 2007a, 2007b); as such, they were once considered an odd and rare occurrence. These materials are now recognized in HiRISE and CTX images of over 200 craters with additional identifications of more pitted-material bearing craters steadily increasing as MRO continues to image the martian surface. As a result, pitted materials represent a newly recognized widespread crater-related geologic unit.

Although the exact nature of these materials and the mechanisms responsible for pit formation are not presently well understood, we conclude based on morphologic and stratigraphic characteristics, that they are consistent with an impact origin, with the pits possibly representing degassing pipes. As such, we contend that the pitted materials are primary impactite deposits that represent the very top of the crater-fill deposits. We suggest that craters exhibiting abundant quasi-circular features or arcuate ridges on their floors may actually be remnants of pitted materials and are not necessarily degraded primaries or secondaries. Careful examinations and comparisons with the results of this study should be used to distinguish remnant-pitted materials from other features and deposits. The crater-related pitted materials are of great significance as they can be used as, (1) a chronologic marker (e.g., like that of lunar rayed craters as the Copernican Era on the Moon), (2) a stratigraphic level to base estimates of bulk erosion and deposition (e.g., Bleacher et al., 2003; Howard, 2007), (3) a tool towards additional insights into the properties and subsurface structure of the pre-impact target, (4) a criterion for crater preservation that can in turn be used to improve constraints on quantitative modeling and crater scaling relationships (diameter vs. depth, peak diameter, pit diameter, number of terraces, terrace spacing, ejecta attributes, etc.), and (5) the focus of future studies to gain insights into the impact process as a geologic process (e.g., distribution and morphometry of various impactites). We provide our database (Table A.1) in the hopes that it will be useful for future studies.

Based on several lines of evidence and inferences from terrestrial and lunar analogs, our preferred hypothesis is that martian crater-related pitted materials represent a mixture of impact melt, volatile-rich materials and mineral and lithic fragments, and that they may be analogous to terrestrial impact-melt bearing breccias as previously suggested by McEwen et al. (2007b) and Tornabene et al. (2007a, 2007b, 2008). Mouginis-Mark and Garbiel (2007) previously suggested the presence of impact melt bodies in Tooting Crater, but reserved the interpretation to only the fractured pit-poor materials in the southern portion of the crater. Our observations show that pits and fractures form together within the same unit, and thereby we suggest that these materials are similar, but may differ in the proportion of "melt" to other components of the deposit including lithic clast and volatile contents. Fractures and pits are also observed to crosscut one another, which suggests that the timing of pit formation and cooling of hot impact melt-rich materials were contemporaneous.

If crater-related pitted materials were emplaced as a hot melt-bearing impact deposit with entrained water, then it is plausible that the pits formed by rapid degassing of volatiles within the deposit in a fashion that is analogous to the formation of degassing structures within the Reis suevite. Regardless of the exact mechanisms involved, it is difficult to explain these features without invoking target volatiles. As such, these crater-related materials now present some of the most tantalizing evidence for volatiles playing a role during the impact process since the discovery of layered ejecta on Mars (Carr et al., 1977). In addition, crater counts indicate that these materials have been forming on Mars throughout most of martian geologic time, and thereby represent an important newly recognized geologic unit on Mars. Because impact melt volume scales with crater diameter, and the frequency of larger impacts being much higher in the past, these materials may represent a major component of the older preserved crusts on Mars. If these materials truly represent volatile-rich impact melts, then the emplacement of numerous and more voluminous hydrous impact melts in the Noachian may have implications for understanding early martian climate, martian valley networks, and the petrogenetic history of the martian crust—including formation of hydrated silicate-bearing lithologies.

Appendix A. Supplementary material

Supplementary data associated with this article can be found, in the online version, at http://dx.doi.org/10.1016/j.icarus.2012.05.022.

References

Banks, M.E. et al., 2010. Crater population and resurfacing of the martian north polar layered deposits. J. Geophys. Res. – Planets 115. http://dx.doi.org/10.1029/2009JE003523.

Barlow, N.G., 2004. Martian subsurface volatile concentrations as a function of time: Clues from layered ejecta craters. Geophys. Res. Lett. 31. http://dx.doi.org/10.1029/2003GL019075.

Barlow, N.G., 2005. A review of martian impact crater ejecta structures and their implications for target properties. In: Kenkmann, T., Hörz, F., Deutsch, A. (Eds.), Large Meteorite Impacts III. Geological Society of America Special Paper 384, pp. 433–442.

Barlow, N.G., Bradley, T.L., 1990. Martian impact craters: correlations of ejecta and interior morphologies with diameter, latitude, and terrain. Icarus 87, 156–179.

Barlow, N.G., Perez, C.B., 2003. Martian impact crater ejecta morphologies as indicators of the distribution of subsurface volatiles. J. Geophys. Res. – Planets 108. http://dx.doi.org/10.1029/2002JE002036.

Barlow, N.G. et al., 2000. Standardizing the nomenclature of martian impact crater ejecta morphologies. J. Geophys. Res. – Planets 105, 26733–26738.

Bleacher, J.E. et al., 2003. Deflation/erosion rates for the Parva Member, Dorsa Argentea Formation and implications for the south polar region of Mars. J. Geophys. Res. – Planets 108. http://dx.doi.org/10.1029/2001JE001535.
Bourke, M.C. et al., 2010. Extraterrestrial dunes: An introduction to the special issue on planetary dune systems. Geomorphology 121. http://dx.doi.org/10.1016/j.geomorph.2010.04.007.
Boyce, J.M., Garbeil, H., 2007. Geometric relationships of pristine martian complex impact craters, and their implications to Mars geologic history. Geophys. Res. Lett. 34. http://dx.doi.org/10.1029/2007GL029731.
Boyce, J.M., Mouginis-Mark, P., 2006. Martian craters viewed by the Thermal Emission Imaging System instrument: Double-layered ejecta craters. J. Geophys. Res. – Planets 111. http://dx.doi.org/10.1029/2005JE002638.
Boyce, J.M. et al., 2006. Deep impact craters in the Isidis and southwestern Utopia Planitia regions of Mars: High target material strength as a possible cause. Geophys. Res. Lett. 33. http://dx.doi.org/10.1029/2005GL024462.
Boyce, J.M., Barlow, N.G., Tornabene, L.L., 2008. Lonar Crater on Mars: Implications of its unusual morphology. Lunar Planet. Sci. XXXIX, 1406 (abstract).
Boyce, J.M., et al., 2011. Pitted deposits in fresh impact craters. Lunar Planet. Sci. XLII, 2701 (abstract).
Boyce, J.M. et al., 2012a. Origin of closely-spaced groups of pits in martian craters. Lunar Planet. Sci. XLIII, 1017 (abstract).
Boyce, J.M. et al., 2012b. Origin of pits in martian impact craters. Icarus, submitted for publication.
Bray, V.J. et al., 2010. New insight into lunar impact melt mobility from the LRO camera. Geophys. Res. Lett. 37. http://dx.doi.org/10.1029/2010GL044666.
Bridges, N.T. et al., 2007. Windy Mars: A dynamic planet as seen by the HiRISE camera. Geophys. Res. Lett. 34. http://dx.doi.org/10.1029/2007GL031445.
Burr, D.M. et al., 2009. Mesoscale raised rim depressions (MRRDs) on Earth: A review of the characteristics, processes, and spatial distributions of analogs for Mars. Planet. Space Sci. 57, 5. http://dx.doi.org/10.1016/j.pss.2008.11.011.
Carr, M.H., 2006. The Surface of Mars. Cambridge Univ Press, New York, 307pp.
Carr, M.H. et al., 1977. Martian impact craters and emplacement of ejecta by surface flow. J. Geophys. Res. 82, 4055–4065.
Christensen, P.R. et al., 2001. Mars Global Surveyor Thermal Emission Spectrometer experiment: Investigation description and surface science results. J. Geophys. Res. – Planets 106, 23823–23871.
Christensen, P.R. et al., 2004. The thermal emission imaging system (THEMIS) for the Mars 2001 Odyssey Mission. Space Sci. Rev. 110, 85–130.
Christensen, P.R. et al., 2009. JMARS: A planetary GIS. American Geophysical Union (Fall Meet.). Abstract IN22A-06.
Cintala, M.J., Grieve, R.A.F., 1998. Scaling impact-melt and crater dimensions: Implications for the lunar cratering record. Meteorit. Planet. Sci. 33, 889–912.
Clifford, S.M., 1993. A model for the hydrologic and climatic behavior of water on Mars. J. Geophys. Res. – Planets 98. http://dx.doi.org/10.1029/1993JE00225.
Clifford, S.M. et al., 2010. Depth of the martian cryosphere: Revised estimates and implications for the existence and detection of subpermafrost groundwater. J. Geophys. Res. – Planets 115. http://dx.doi.org/10.1029/2009JE003462.
Craddock, R., Maxwell, T., Howard, A., 1997. Crater morphometry and modification in the Sinus Sabaeus and Margaritifer Sinus regions of Mars. J. Geophys. Res. – Planets 102, 13321–13340.
Delamere, W.A. et al., 2010. Color imaging of Mars by the High Resolution Imaging Science Experiment (HiRISE). Icarus 205, 38–52.
Edgett, K.S., 2005. The sedimentary rocks of Sinus Meridiani: Five key observations from data acquired by the Mars Global Surveyor and Mars Odyssey orbiters. Mars 1. http://dx.doi.org/10.1555/mars.2005.0002.
Edgett, K.S., Blumberg, D.G., 1994. Star and linear dunes on Mars. Icarus 112. http://dx.doi.org/10.1006/icar.1994.1197.
Fagents, S.A., Thordarson, T., 2007. Rootless volcanic cones in Iceland and on Mars. In: Chapman, M.G. (Ed.), The Geology of Mars: Evidence from Earth-Based Analog. Cambridge University Press, Cambridge, UK, pp. 151–177.
Forsberg-Taylor, N.K., Howard, A.D., Craddock, R.A., 2004. Crater degradation in the martian highlands: Morphometric analysis of the Sinus Sabaeus region and simulation modeling suggest fluvial processes. J. Geophys. Res. – Planets 109. http://dx.doi.org/10.1029/2004JE002242.
Garvin, J.B., Sakimoto, S.E.H., Frawley, J.J., 2003. Craters on Mars: Global geometric properties from gridded MOLA topography. In: Sixth International Conference on Mars, Pasadena, CA. 3277 (abstract).
Ghent, R.R., Anderson, S.W., Pthwala, T.M., 2012. The formation of small cones in Isidis Planitia, Mars through mobilization of pyroclastic surge deposits. Icarus 217. http://dx.doi.org/10.1016/j.icarus.2011.10.018.
Gorelick, N.S. et al., 2003. JMARS: A multi-mission data fusion application. Lunar Planet. Sci. XXXIV, 2057 (abstract).
Grant, J.A. et al., 2008. Degradation of Victoria Crater, Mars. J. Geophys. Res. – Planets 113. http://dx.doi.org/10.1029/2008JE003155.
Greeley, R., Guest, J.E., 1986. Geological Map of the Western Equatorial Region of Mars. US Geol. Surv. Scientific Investigations, I-1802-B.
Grieve, R.A.F., 1988. The Haughton impact structure – Summary and synthesis of the results of the HISS project. Meteorit. Planet. Sci. 23, 249–254.
Grieve, R.A.F., Cintala, M.J., 1992. An analysis of differential impact crater scaling and implications for the terrestrial record. Meteorit. Planet. Sci. 27, 526–538.
Grieve, R.A.F., Dence, M.R., Robertson, P.B., 1977. Cratering processes: As interpreted from the occurrence of impact melts. In: Roddy, D.J., Pepin, R.O., Merrill, R.B. (Eds.), Impact and Explosion Cratering. Pergamon Press, New York, pp. 791–814.
Hamilton, C.W., Thordarson, T., Fagents, S.A., 2010a. Explosive lava–water interactions I: Architecture and emplacement chronology of volcanic rootless cone groups in the 1783–1784 Laki lava flow. Bull. Volcanol. 72. http://dx.doi.org/10.1007/s00445-009-0330-6.
Hamilton, C.W., Fagents, S.A., Thordarson, T., 2010b. Explosive lava–water interaction II: Self-organization processes among volcanic rootless eruption sites in the 1783–1784 Laki lava flow, Iceland. Bull. Volcanol. 72. http://dx.doi.org/10.1007/s00445-009-0331-5.
Hamilton, C.W., Fagents, S.A., Wilson, L., 2010c. Explosive lava–water interactions in Elysium Planitia, Mars: Constraints on the formation of the Tartarus Colles cone groups. J. Geophys. Res. – Planets 115. http://dx.doi.org/10.1029/2009JE003546.
Hamilton, C.W., Fagents, S.A., Thordarson, T., 2011. Lava–ground ice interactions in Elysium Planitia, Mars: Geomorphological and geospatial analysis of the Tartarus Colles cone groups. J. Geophys. Res. – Planets 116. http://dx.doi.org/10.1029/2010JE003657.
Harrison, T.N. et al., 2010. Impact-induced overland fluid flow and channelized erosion at Lyot Crater, Mars. Geophys. Res. Lett. 37. http://dx.doi.org/10.1029/2010GL045074.
Hartmann, W.K., 2005. Martian cratering 8: Isochron refinement and the chronology of Mars. Icarus 174, 294–320.
Hartmann, W.K. et al., 2010. Do young martian ray craters have ages consistent with the crater count system? Icarus 208. http://dx.doi.org/10.1016/j.icarus.2010.03.030.
Hawke, B.R., Head, J.W., 1977. Impact melt on lunar crater rims. In: Roddy, D.J., Pepin, R.O., Merrill, R.B. (Eds.), Impact and Explosion Cratering. Pergamon Press, New York, pp. 815–841.
Heather, D.J., Dunkin, S.K., 2003. Geology and stratigraphy of King Crater, lunar farside. Icarus 163. http://dx.doi.org/10.1016/S0019-1035(02)00063-5.
Howard, A.D., 2007. Simulating the development of martian highland landscapes through the interaction of impact cratering, fluvial erosion, and variable hydrologic forcing. Geomorphology 91. http://dx.doi.org/10.1016/j.geomorph.2007.04.017.
Jaeger, W.L., Keszthelyi, L.P., McEwen, A.S., Dundas, C.M., Russell, P.S., 2007. Athabasca Valles, Mars: A Lava-draped channel system. Science 317, 1709–1711.
Jones, A.P., Claeys, P., Heuschkel, S., 2000. Impact melting: A review of experimental constraints for carbonate targets and applications to the Chicxulub crater. In: Gilmour I., Koeberl C. (Eds.), Impact and Early Earth, Springer-Verlag, Berlin. Lecture Notes in Earth Sciences 91, pp. 343–362.
Jones, A.P. et al., 2011. A geomorphic analysis of Hale Crater, Mars: The effects of impact into ice-rich crust. Icarus 211. http://dx.doi.org/10.1016/j.icarus.2010.10.014.
Kadish, S.J. et al., 2008. Martian pedestal craters: Marginal sublimation pits implicate a climate-related formation mechanism. Geophys. Res. Lett. 35. http://dx.doi.org/10.1029/2008GL034990.
Keszthelyi, L., et al., 2008. High Resolution Imaging Science Experiment (HiRISE) images of volcanic terrains from the first 6 months of the Mars Reconnaissance Orbiter Primary Science Phase. J. Geophys. Res. 113, E04005. http://dx.doi.org/10.1029/2007JE002968.
Kirk, R.L. et al., 2008. Ultrahigh resolution topographic mapping of Mars with MRO HiRISE stereo images: Meter-scale slopes of candidate Phoenix landing sites. J. Geophys. Res. – Planets 113. http://dx.doi.org/10.1029/2007JE003000.
Korteniemi, J., Kreslavsky, M.A, 2011. Northern patterned ground margin on Mars: terrain types and age estimates. Lunar Planet. Sci. XLII, 2519 (abstract).
Lang, N.P. et al., 2009. Tharsis-sourced relatively dust-free lavas and their possible relationship to martian meteorites. J. Volcanol. Geoth. Res. http://dx.doi.org/10.1029/2009JE003397.
Lucchitta, B.K., 1981. Mars and Earth: Comparison of cold-climate features. Icarus 45 (2), 264–303.
Malin, M.C., Edgett, K.S., 2001. Mars Global Surveyor Mars Orbiter Camera: Interplanetary cruise through primary mission. J. Geophys. Res. – Planets 110, 23429–23570.
Malin, M.C. et al., 2007. Context camera investigation on board the Mars Reconnaissance Orbiter. J. Geophys. Res. – Planets 112. http://dx.doi.org/10.1029/2006JE002808.
McEwen, A.S. et al., 2005. The rayed crater Zunil and interpretations of small impact craters on Mars. Icarus 176, 351–381.
McEwen, A.S. et al., 2007a. Mars Reconnaissance Orbiter's High Resolution Imaging Science Experiment (HiRISE). J. Geophys. Res. – Planets 112. http://dx.doi.org/10.1029/2005JE002605.
McEwen, A.S. et al., 2007b. A closer look at water-related geologic activity on Mars. Science 317. http://dx.doi.org/10.1126/science.1143987.
McEwen, A.S. et al., 2010. The High Resolution Imaging Science Experiment (HiRISE) during MRO's Primary Science Phase (PSP). Icarus 205. http://dx.doi.org/10.1016/j.icarus.2009.04.023.
Mellon, M.T., Jakosky, B.M., 1995. The distribution and behavior of martian ground ice during past and present epochs. J. Geophys. Res. – Planets 100, 11781–11799.
Mellon, M.T., Jakosky, B.M., Postawko, S.E., 1997. The persistence of equatorial ground ice on Mars. J. Geophys. Res. – Planets 102, 19357–19369.
Melosh, H.J., 1989. Impact Cratering. Oxford University Press, New York, 245pp.
Morris, A.R., Mouginis-Mark, P.J., 2006. Thermally distinct craters near Hrad Vallis, Elysium Planitia, Mars. Icarus 180, 335–347.
Morris, A.R., Mouginis-Mark, P.J., Garbeil, H., 2010. Possible impact melt and debris flows at Tooting Crater, Mars. Icarus 209. http://dx.doi.org/10.1016/j.icarus.2010.05.029.

Mouginis-Mark, P.J., Boyce, J.M., 2012. Tooting Crater: Geology and geomorphology of the archetype fresh, large crater on Mars. Chem. Erde Geochem. 72. http://dx.doi.org/10.1016/j.chemer.2011.12.001.

Mouginis-Mark, P.J., Garbiel, H., 2007. Crater geometry and ejecta thickness of the martian impact crater Tooting. Meteorit. Planet. Sci. 42, 1615–1625.

Moyer, T.C., Swanson, D.A., 1987. Secondary hydroeruptions in pyroclastic-flow deposits: Examples from Mount St. Helens. J. Volcanol. Geotherm. Res. 32, 299–319.

Mustard, J.F., Cooper, C.D., Rifkin, K.R., 2001. Evidence for recent climate change on Mars from identification of youthful near-surface ground ice. Nature 412, 411–413.

Newsom, H.E. et al., 1986. Fludization and hydrothermal alteration of the Suevite Deposit at the Ries Crater, West Germany, and Implications for Mars. Proc. Lunar Sci. Conf. 17, 239–251.

Okubo, C.H., Martel, S.J., 1998. Pit crater formation on Kilauea volcano, Hawaii. J. Volcanol. Geoth. Res. 86, 1–18.

Osinski, G.R., 2003. Impact glasses in fallout suevites from the Ries impact structure, Germany: An analytical SEM study. Meteorit. Planet. Sci. 38, 1641–1667.

Osinski, G.R., 2004. Impact melt rocks from the Ries structure, Germany: an origin as impact melt flows? Earth Planet. Sci. Lett. 226, 529–543.

Osinski, G.R., Tornabene, L.L., Grieve, R.A.F., 2011. Impact melt and ejecta emplacement on terrestrial planets. Earth Planet. Sci. Lett. http://dx.doi.org/10.1016/j.epsl.2011.08.012.

Pathare, A.V., Paige, D.A., Turtle, E.P., 2005. Viscous relaxation of craters within the martian south polar layered deposits. Icarus 174, 396–418.

Pierce, T.L., Crown, D.A., 2003. Morphologic and topographic analyses of debris aprons in the eastern Hellas region, Mars. Icarus. 163, 46–65.

Pope, K.O., Kieffer, S.W., Ames, D.E., 2007. Impact melt sheet formation on Mars and its implication for hydrothermal systems and exobiology. Icarus 183, 1–9.

Preblich, B., McEwen, A., Studer, D., 2007. Mapping rays and secondary craters from Zunil, Mars. J. Geophys. Res. – Planets 112. http://dx.doi.org/10.1029/2006JE002817.

Rowland, S.K., Mouginis-Mark, P.J., Fagents, S.A., 2011. NASA volcanology field workshops on Hawai'i: Part 1. Description and history. In: Garry, W.B., Bleacher J.E. (Eds.), Analogs for Planetary Exploration: GSA Special Paper 483, pp. 401–434. http://dx.doi.org/10.1130/2011.2483(25).

Ruff, S.W., Christensen, P.R., 2002. Bright and dark regions on Mars: Particle size and mineralogical characteristics based on Thermal Emission Spectrometer data. J. Geophys. Res. – Planets 107. http://dx.doi.org/10.1029/2001JE001580.

Schon, S.C., Head, J.W., 2011. Keys to gully formation processes on Mars: Relation to climate cycles and sources of meltwater. Icarus 213, 428–432.

Schon, S.C., Head, J.W., Fassett, C.I., 2009. Unique chronostratigraphic marker in depositional fan stratigraphy on Mars: Evidence for ca. 1.25 Ma gully activity and surficial meltwater origin. Geology 2009 (37), 207–210.

Scott, D.H., Tanaka, K.L., 1986. Geological map of the western equatorial region of Mars. US Geol. Surv. Scientific Investigations, I-1802-A.

Searls, M.L. et al., 2008. Slope analysis and ice stability of the mid latitude dissected terrain on Mars. Lunar Planet. Sci. XXXIX, 2376 (abstract).

Skinner Jr., J.A., Tanaka, K.L., 2007. Evidence for and implications of sedimentary diapirism and mud volcanism in the southern Utopia highland–lowland boundary plain, Mars. Icarus 186, 41–59.

Skinner, J.A., Hare, T.M., Tanaka, K.L., 2006. Digital renovation of the atlas of Mars 1:15,000,000-scale global geologic series maps. Lunar Planet. Sci. XXXVII, 2331 (abstract).

Smith, D.E. et al., 2001. Mars Orbiter Laser Altimeter: Experiment summary after the first year of global mapping of Mars. J. Geophys. Res. – Planets 106, 23689–23722.

Soare, R.J. et al., 2007. Thermokarst processes and the origin of crater-rim gullies in Utopia and western Elysium Planitia. Icarus 191, 95–112.

Soare, R.J., Osinski, G.R., Roehm, C.L., 2008. Thermokarst lakes and ponds on Mars in the very recent (late Amazonian) past. Earth Planet. Sci. Lett. 272, 382–393.

Squyres, S.W. et al., 1992. Ice in the martian regolith. In: Kieffer, H.H., Jakosky, B.M., Snyder, C.W., Matthews, M.S. (Eds.), Mars. Univ. of Ariz Press, Tucson, pp. 523–554.

Stewart, S.T., Valiant, G.J., 2006. Martian subsurface properties and crater formation processes inferred from fresh impact crater geometries. Meteorit. Planet. Sci. 41, 1509–1537.

Stöffler, D., Grieve, R.A.F., 2007. Impactites (Chapter 2.11 Metamorphic rocks: A classification, and glossary of terms). In: Fettes, D., Desmons, J. (Eds.), Recommendations of the International Union of Geological Sciences. Cambridge University Press, Cambridge, pp. 82–92, 111–125, and 126–242, respectively.

Tornabene, L.L. et al., 2006. Identification of large (2–10 km) rayed craters on Mars in THEMIS thermal infrared images: Implications for possible martian meteorite source regions. J. Geophys. Res. – Planets 111. http://dx.doi.org/10.1029/2005JE002600.

Tornabene, L.L. et al., 2007a. Evidence for the role of volatiles on martian impact craters as revealed by HiRISE. Lunar Planet. Sci. XXXVIII, 2215 (abstract).

Tornabene, L.L. et al., 2007b. Impact melting & the role of sub-surface volatiles: Implications for the formation of valley networks & phyllosilicate-rich lithologies on early Mars. In: Seventh International Conference on Mars, 3288 (abstract).

Tornabene, L.L. et al., 2008. Recent channel systems emanating from Hale Crater Ejecta: Implications for the Noachian landscape evolution of Mars. Lunar Planet. Sci. XXXIX, 2180 (abstract).

Williams, R.M.E., Malin, M.C., 2008. Sub-kilometer fans in Mojave Crater, Mars. Icarus 198. http://dx.doi.org/10.1016/j.icarus.2008.07.013.

Wyrick, D., Ferrill, D.A., 2004. Distribution, morphology, and origins of martian pit crater chains. J. Geophys. Res. – Planets 109. http://dx.doi.org/10.1029/2004JE002240.

Zurek, R.W., Smrekar, S.E., 2007. An overview of the Mars Reconnaissance Orbiter (MRO) science mission. J. Geophys. Res. – Planets 112. http://dx.doi.org/10.1029/2006JE002701.